

Community assessment to advance computational prediction of cancer drug combinations in a pharmacogenomic screen

Menden, Michael P.; Wang, Dennis; Mason, Mike J.; Szalai, Bence; Bulusu, Krishna C.; Guan, Yuanfang; Yu, Thomas; Aben, Nanne; Wessels, Lodewyk; More Authors

DOI

[10.1038/s41467-019-09799-2](https://doi.org/10.1038/s41467-019-09799-2)

Publication date

2019

Document Version

Final published version

Published in

Nature Communications

Citation (APA)

Menden, M. P., Wang, D., Mason, M. J., Szalai, B., Bulusu, K. C., Guan, Y., Yu, T., Aben, N., Wessels, L., & More Authors (2019). Community assessment to advance computational prediction of cancer drug combinations in a pharmacogenomic screen. *Nature Communications*, *10*(1), Article 2674. <https://doi.org/10.1038/s41467-019-09799-2>

Important note

To cite this publication, please use the final published version (if applicable). Please check the document version above.

Copyright

Other than for strictly personal use, it is not permitted to download, forward or distribute the text or part of it, without the consent of the author(s) and/or copyright holder(s), unless the work is under an open content license such as Creative Commons.

Takedown policy










Please contact us and provide details if you believe this document breaches copyrights. We will remove access to the work immediately and investigate your claim.

ARTICLE

<https://doi.org/10.1038/s41467-019-09799-2>

OPEN

Community assessment to advance computational prediction of cancer drug combinations in a pharmacogenomic screen

Michael P. Menden ^{1,2,185,187}, Dennis Wang^{1,3,187}, Mike J. Mason ^{4,187}, Bence Szalai^{5,6,7,187}, Krishna C. Bulusu^{1,187}, Yuanfang Guan^{8,187}, Thomas Yu ⁴, Jaewoo Kang ⁹, Minji Jeon⁹, Russ Wolfinger¹⁰, Tin Nguyen ¹¹, Mikhail Zaslavskiy¹², AstraZeneca-Sanger Drug Combination DREAM Consortium[†], In Sock Jang⁴, Zara Ghazoui¹, Mehmet Eren Ahsen ¹³, Robert Vogel¹³, Elias Chaibub Neto⁴, Thea Norman⁴, Eric K.Y. Tang¹, Mathew J. Garnett¹⁴, Giovanni Y. Di Veroli¹⁵, Stephen Fawell¹⁶, Gustavo Stolovitzky ^{13,17}, Justin Guinney ^{4,188}, Jonathan R. Dry^{16,188} & Julio Saez-Rodriguez ^{2,7,186,188}

The effectiveness of most cancer targeted therapies is short-lived. Tumors often develop resistance that might be overcome with drug combinations. However, the number of possible combinations is vast, necessitating data-driven approaches to find optimal patient-specific treatments. Here we report AstraZeneca's large drug combination dataset, consisting of 11,576 experiments from 910 combinations across 85 molecularly characterized cancer cell lines, and results of a DREAM Challenge to evaluate computational strategies for predicting synergistic drug pairs and biomarkers. 160 teams participated to provide a comprehensive methodological development and benchmarking. Winning methods incorporate prior knowledge of drug-target interactions. Synergy is predicted with an accuracy matching biological replicates for >60% of combinations. However, 20% of drug combinations are poorly predicted by all methods. Genomic rationale for synergy predictions are identified, including ADAM17 inhibitor antagonism when combined with PIK3CB/D inhibition contrasting to synergy when combined with other PI3K-pathway inhibitors in PIK3CA mutant cells.

¹Oncology, IMED Biotech Unit, AstraZeneca, Cambridge SG8 6EH, UK. ²European Bioinformatics Institute, European Molecular Biology Laboratory, Cambridge CB10 1SD, UK. ³Sheffield Institute for Translational Neuroscience, University of Sheffield, Sheffield S10 2TN, UK. ⁴Sage Bionetworks, Seattle, WA 98121, USA. ⁵Department of Physiology, Faculty of Medicine, Semmelweis University, Budapest 1085, Hungary. ⁶Laboratory of Molecular Physiology, Hungarian Academy of Sciences and Semmelweis University (MTA-SE), Budapest 1085, Hungary. ⁷RWTH Aachen University, Faculty of Medicine, Joint Research Center for Computational Biomedicine, Aachen 52062, Germany. ⁸Department of Computational Medicine and Bioinformatics, University of Michigan, Ann Arbor 48109, USA. ⁹Department of Computer Science and Engineering, Korea University, Seoul 02841, Korea. ¹⁰SAS Institute, Inc, Cary, NC 27513, USA. ¹¹Department of Computer Science and Engineering, University of Nevada, Reno 89557, USA. ¹²Independent Consultant in Computational Biology, Owkin, Inc., New York, NY 10022, USA. ¹³IBM Thomas J. Watson Research Center, Yorktown Heights, New York 10598, USA. ¹⁴Wellcome Trust Sanger Institute, Hinxton CB10 1SA, UK. ¹⁵Early Clinical Development, IMED Biotech Unit, AstraZeneca, Cambridge SG8 6EH, UK. ¹⁶Oncology, IMED Biotech Unit, AstraZeneca, R&D Boston, Waltham, MA 02451, USA. ¹⁷Department of Genetics and Genomic Sciences, Icahn School of Medicine at Mount Sinai, New York 10029, USA. ¹⁸⁵Present address: Institute of Computational Biology, Helmholtz Zentrum München - German Research Center for Environmental Health, Munich D-85764, Germany. ¹⁸⁶Present address: Heidelberg University, Faculty of Medicine, Institute for Computational Biomedicine, Bioquant, 69120 Heidelberg, Germany. ¹⁸⁷These authors contributed equally: Michael P. Menden, Dennis Wang, Mike J. Mason, Bence Szalai, Krishna C. Bulusu, Yuanfang Guan. ¹⁸⁸These authors jointly supervised this work: Justin Guinney, Jonathan R. Dry, Julio Saez-Rodriguez. [†]A full list of consortium members appears at the end of the paper. Correspondence and requests for materials should be addressed to J.G. (email: justin.guinney@sagebionetworks.org) or to J.R.D. (email: jonathan.dry@astrazeneca.com) or to J.S.-R. (email: julio.saez@bioquant.uni-heidelberg.de)

Personalized treatment matching targeted drugs to a tumor's genetics has resulted in remarkable responses. Unfortunately, most patients' tumors develop resistance leading to disease relapse. There are multiple mechanisms that may lead to drug resistance¹ that include genetic and non-genetic heterogeneity inherent in advanced cancers, coupled with complex feedback and regulatory mechanisms, and dynamic interactions between tumor cells and their microenvironment. Any single therapy may be limited in its effectiveness, but drug combinations are hypothesized to potentially overcome drug resistance and lead to more durable responses in patients. The molecular makeup of cancer cells and the mechanisms driving resistance will influence the optimal combination of mechanisms to target¹⁻³.

High-throughput preclinical approaches are crucial to determine and evaluate effective combination strategies. While empirical experiments are important for observing potential synergistic properties across drug pairs, the possible number of combinations grows exponentially with the number of drugs under consideration. This is further complicated by the influence of disease and cellular contexts, rendering it impractical to cover all possibilities with undirected experimental screens⁴. Computational approaches for predicting drug synergy are critical to guide experimental approaches for discovery of rational combination therapy⁵.

A number of approaches have been developed to model drug combination synergy using chemical, biological, and molecular data from cancer cell lines^{6,7} but with limited translatability to the clinic. A key bottleneck in the development of such models has been a lack of public data of sufficient size and variety to train computational approaches^{4,8}, particularly considering the diversity of biological mechanisms that may influence drug response. A further limit to the translatability of many computational approaches is their reliance on data features that may not be present during the course of patient care, such as on-treatment tumor molecular profiles.

To accelerate the understanding of drug combination synergy, Dialog for Reverse Engineering Assessments and Methods (DREAM) Challenges partnered with AstraZeneca and the Sanger Institute to launch the AstraZeneca-Sanger Drug Combination Prediction DREAM Challenge. DREAM Challenges (dreamchallenges.org/www.dreamchallenges.org) are collaborative competitions that pose important biomedical questions to the scientific community, and evaluate participants' predictions in a statistically rigorous and unbiased way, emphasizing model reproducibility, and methodological transparency⁹.

This Challenge was designed to explore fundamental traits that underlie effective combination treatments and synergistic drug behavior. Specifically, it was structured to address the following translational questions using data available prior to drug treatment (mirroring a clinically relevant scenario to direct therapeutic choice): [i] how to predict whether a known (previously tested) drug combination will be effective for a specific patient; [ii] how to predict which new (untested) drug combinations are likely to yield synergistic behaviors in a patient population; and [iii] how to identify novel biomarkers that may help reveal underlying mechanisms related to drug synergy.

We shared with the scientific community 11,576 experimentally tested drug combinations on 85 cancer cell lines. Molecular data was provided for the untreated (baseline) cell lines, alongside chemical information for the respective drugs. Participants used the described data to train and test models, and were encouraged to extend computational techniques to leverage a priori knowledge of cellular signaling networks.

In this manuscript, we report on the results of this Challenge where we have identified novel and performant methods using a rigorous evaluation framework on previously unpublished data.

We describe the details of these approaches, as well as general trends arising from the meta-analysis of all submissions. The full dataset, along with methods and scoring functions, are freely provided to the research community, and available to benchmark future algorithms in the field. Finally, we describe putative mechanistic models derived from the observed predictive features underlying synergistic responses, particularly between receptor tyrosine kinase and PI3K/AKT pathway inhibitors.

Results

A large high-throughput drug combination screen. We collated a combinatorial drug sensitivity screen comprising 11,576 experiments each measured in a 6-by-6 dose matrix (Methods) across 85 cancer cell lines. A synergy and an antagonism distribution (Loewe reference model^{10,11}) were calculated and summarized via a single score for each experimental matrix (Methods; Supplementary Fig. 1 and Supplementary Data 1). The resulting dataset included highly reproducible cell viability response measurements and synergy scores for 910 pairwise combinations of 118 drugs (Supplementary Fig. 2 and Methods), plus information on the drugs including putative drug targets and their chemical properties. We also integrated deep molecular characterization of these same cell lines, including somatic mutations, copy-number alterations, DNA methylation, and gene expression profiles (Fig. 1a-c) measured before drug treatment¹².

The 85 cell lines were predominantly derived from tumors of the breast ($N = 34$), lung ($N = 22$), bladder ($N = 14$), and the gastrointestinal tract ($N = 12$) (Fig. 1d). Drug synergy score distributions varied across disease types (Fig. 1d); in particular lung cell lines had over twofold higher mean synergy than breast cell lines (t -test $P = 7e-27$). Of the 118 drugs tested, 59 were targeted therapies against components of oncogenic signaling pathways (Methods), 15 of which target receptor tyrosine kinases (RTKs), 22 target PI3K/AKT signaling, and 9 target MAPK signaling (Fig. 1e, f). Across the pairwise drug combination experiments, 88% ($N = 797$) of the unique pairs had drug targets within the same signaling pathway and demonstrated markedly overall higher synergy scores (average of 17.3 vs. 7.3, t -test $P = 2e-18$) than the remaining 12% ($N = 113$) whose drug targets were defined to be in distinct pathways. As part of the Challenge design, we ensured that drug targeted pathways and cancer types were proportionally distributed across sub-challenges and training/test datasets (Fig. 1g). Sparsity in the cell line drug combination data matrix (Fig. 1g) resulted as several drug combinations were selectively profiled in clinically relevant cancer cell lines, e.g., ESR1 inhibitors were predominantly combined with other drugs in estrogen receptor-positive breast cancer cell lines since these agents are standard of care within this cancer subtype.

Comparison of AZ-DREAM to published combination screens.

We compared the AstraZeneca-DREAM (AZ-DREAM) challenge dataset with the independently published in vitro combination screening studies by O'Neil et al.⁴ and ALMANAC¹³. All three studies used different experimental designs and protocols (Fig. 2a and Supplementary Table 1), with AZ-DREAM exploring screens with a 5-by-5 concentration titration format, O'Neil et al.⁴ a 4-by-4 format, and ALMANAC a 3-by-3 format. The overlap is limited in cell lines, targets and drugs explored: 10 cells and 7 targets, 4 drugs and 0 combination-cell pairs shared between AZ-DREAM and O'Neil et al.⁴; and 15 cells, 28 targets, 19 drugs, and 10 combination-cell pairs shared between AZ-DREAM and ALMANAC. AZ-DREAM provides greater coverage of targeted agents and greater numbers of cell lines per tumor type (Supplementary Table 1).

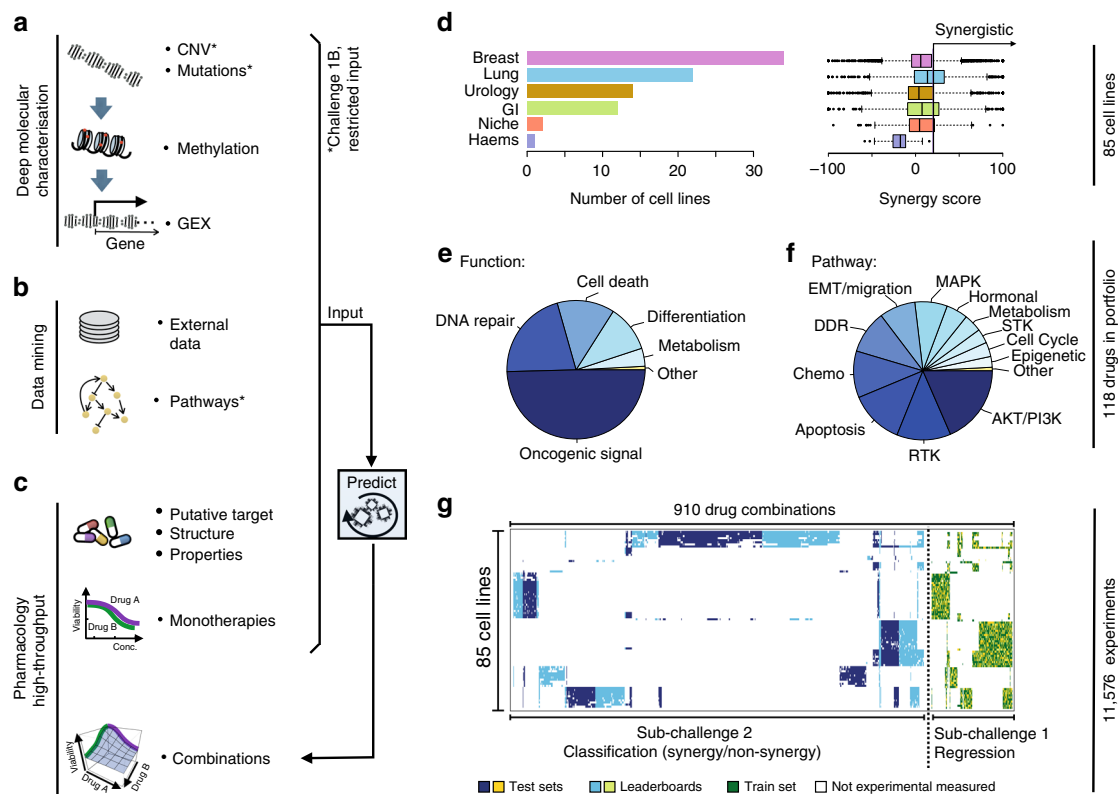


Fig. 1 Drug combinations and cell lines profiled. **a** Molecular characterization of the cell lines included genetics, epigenetics, and transcriptomics. **b** Participants were encouraged to mine external data and pathway resources. **c** Participants were provided the putative targets for all and chemical structures for $\sim 1/3$ of drugs (with this manuscript structures are now provided for all drugs). **d** The cell line panel contained 85 cell lines from six different cancer types, combination synergy scores capped within a range of -100 to 100 . **e** The drug portfolio comprised approximately half oncogenic signaling targeting agents, and half cytotoxic drugs of which 14 were untargeted chemotherapies. **f** Drugs split by the putative targeted pathway. **g** Sparse data was split into training set, leaderboard, and independent test set for SC1 and SC2

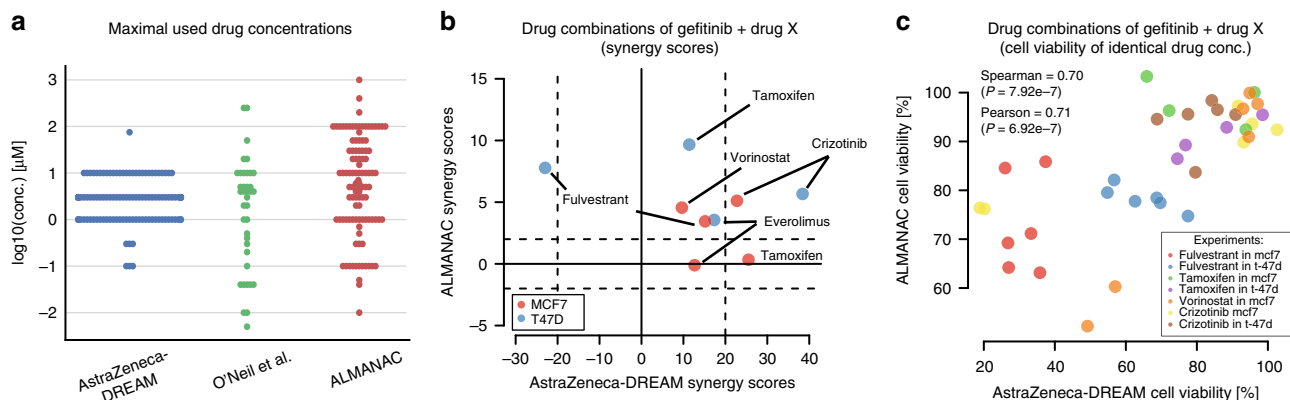


Fig. 2 Reproducibility of independent in vitro drug combination datasets. **a** Comparison of the maximum drug concentration used in the AZ-DREAM, O'Neil et al.⁴ and ALMANAC datasets. **b** Synergy scores of identical drug combinations in AZ-DREAM and ALMANAC. Horizontal and vertical striped lines mark the threshold for synergistic and antagonistic, where positive and negative scores confirm synergy and antagonism, respectively. **c** Shows cell viability for each of the 38 overlapping experimental titration points that are identical in AZ-DREAM and ALMANAC across the nine drug combination experiments, significance calculated with test for association (Supplementary Fig. 3)

For the AZ-DREAM and ALMANAC comparison, only nine experiments passing quality control (Supplementary Methods) had the same combination tested in the same cell line, comprising gefitinib combined with either tamoxifen, fulvestrant, vorinostat, crizotinib, or everolimus, and tested in two breast cancer cell lines (MCF7 or T47D). Encouragingly, all but one experiment were concordantly identified synergistic with the same effect signs seen

in AZ-DREAM and ALMANAC (Fig. 2b). Within the nine overlapping experiments, 38 titrations were identically used by both ALMANAC and AZ-DREAM (Supplementary Fig. 3 and Supplementary Fig. 4a). For these 38 titrations we observed a correlation >0.7 (Fig. 2c and $P < 10^{-7}$, test for association) between cell viability measures from AZ-DREAM and ALMANAC, maintained for individual combinations and cell lines

where the number of data points was sufficient (Supplementary Fig. 4).

While there were ten cell lines and four drugs found in both AZ-DREAM and O'Neil et al.⁴, no combination-cell experiment was shared between those two screens. O'Neill et al.⁴ data displayed lower dispersion of synergy scores (Supplementary Fig. 2c, d) and fewer instances of extreme synergy scores. The technical reproducibility within these screens, however, was comparable, with a similar correlation observed between replicated experiments (Spearman = 0.63 for O'Neil et al.,⁴ Spearman = 0.56 for AZ-DREAM).

We derived a RECIST-like response measure from the AZ-DREAM in vitro data (see Methods) to enable comparison to in vivo response metrics for the eight overlapping combinations in patient-derived tumor xenograft (PDX) models published by Gao et al.⁸ (Supplementary Data 1 and Supplementary Fig. 5a). We compared the % PDX models with synergy in Gao et al.^{4,8} to the % cell lines with synergy in AZ-DREAM. A concordant trend was observed (Pearson $r = 0.34$, $P = 0.42$; Methods; Supplementary Fig. 5b), although too few combinations were shared between the datasets to conclude with statistical confidence.

Benchmarking of methods reveal high prediction accuracy. The Challenge was divided into two primary sub-challenges. In sub-challenge 1 (SC1) participants were asked to predict continuous synergy scores for drug combinations for which training data on those same combinations were available. In sub-challenge 2 (SC2), participants were asked to predict binary synergy status on drug combinations for which no training data was provided, thereby requiring participants to infer synergy using transferable data/knowledge patterns identified from previously seen

independent drug pairs. SC1 was further subdivided into two parts: SC1A allowed the use of all available data for model prediction, while SC1B limited data use to just mutation and copy-number variation (mimicking current clinical assay feasibility).

A total of 969 participants of diverse geography and expertise registered for the Challenge (Supplementary Fig. 6a, b). One-hundred sixty teams submitted across any portion of the Challenge and 78 teams submitted for final assessment. Specifically, SC1A received final submissions from 76 teams, 62 for SC1B and 39 for SC2.

As scoring metric we used the average weighted Pearson correlation between the continuous endpoints of predicted and known synergy values for SC1, and both the $-\log_{10}(p)$ from a 3-way analysis of variance (ANOVA) and balanced accuracy (BAC) for SC2 where predictions were binary (Methods). Across all teams, mean performance scores were $r = 0.24 \pm 0.01$ and $r = 0.23 \pm 0.01$ (weighted Pearson correlation \pm standard error) for SC1A and SC1B, respectively, and $-\log_{10}(p) = 12.6$ (3-way ANOVA) for SC2. Despite omitting several input data types, teams performed only slightly worse for SC1B, Δ primary metric = 0.01 (t -test $P = 0.90$), compared to SC1A (Fig. 3a and Supplementary Fig. 6c, d). While teams employed many different methodological approaches to modeling drug synergy—including regression, decision trees, random forests, Gaussian processes, SVM, neural networks, text mining, mechanistic network-based, and others (Supplementary Fig. 7a)—algorithm class showed little relationship to performance (Supplementary Fig. 7b). The top winning team in all three sub-challenge was *Yuanfang Guan* (Y Guan) with primary metrics of 0.48, 0.45, and 74.89 in SC1A, SC1B, and SC2, respectively. Based on the primary metric in SC2, Y Guan performed considerably better (Methods; >5 Bayes Factor, based on bootstrapped metrics' comparisons) than other

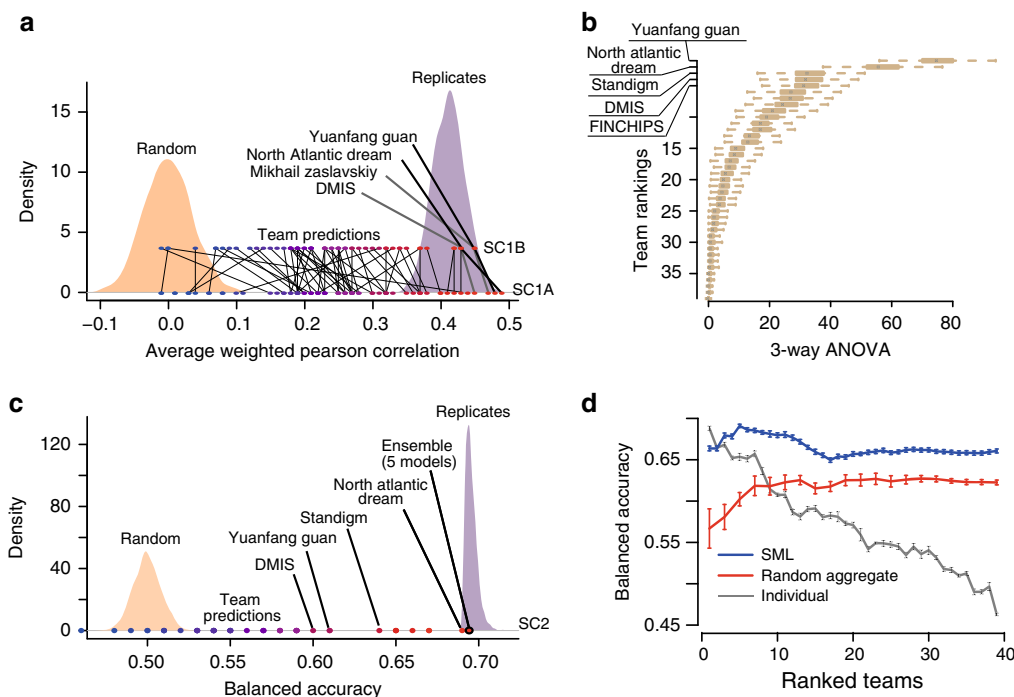


Fig. 3 Performance of teams in the AstraZeneca-DREAM challenge. **a** Participant performance in SC1A and SC1B—the distribution of performance of random predictions was used to estimate a lower limit, and the distribution of synergy correlations between biological replicates were used to estimate the upper limit. **b** Participant performance ranked in SC2 based on the primary metric, 3-way ANOVA. Distribution of bootstrap prediction performances for each team are shown by each boxplot with the dot showing their actual performance. **c** Participant performance plotted with upper and lower limits for SC2 based on the tie-break metric. **d** Ensemble models compared to the performance of individual models ranked from best to poorest performing in SC2. SML is an ensemble of the best performing models based on estimation of their BAC. Random Aggregation is an ensemble combining a random combination of models. Standard error of mean represented by error bars are estimated from ten random splits of the data

teams (Fig. 3b). All performance statistics and team rankings are available at the Challenge website (synapse.org/DrugCombinationChallenge[<https://www.synapse.org/#!Synapse:syn4231880/wiki/235649>]).

To benchmark the performance of teams in the final rounds of SC1A/B and SC2, we established lower and upper bounds of performance. We defined the lower bound as the null model, i.e., random permutation of the synergy data across each cell line (see ‘Code availability’ section). We would not expect algorithms to predict better than the reproducibility observed between replicate experiments. We therefore identified cases for which replicate measurements (same drug/combination tested independently in the same cell line) were available and assessed the primary metric achieved when using one measure to predict the other. We set this metric value as our upper-bound. We observed that 83%, 85%, and 94% of submitted models performed better than random (Methods; 5% false discovery rate, FDR) for SC1A, SC1B, and SC2, respectively. Team performances varied widely, but remarkably the top 15 models (20%) submitted to SC1A all reached a performance level comparable to experimental replicates (primary metric = 0.43; Fig. 3a), as did the top 13 models (21%) in SC1B. Proportionally fewer teams performed at the level of replicate experiments in SC2 based on the BAC, with North Atlantic Dream (NAD) achieving the best performance (BAC = 0.688; Fig. 3c).

Given the less robust performance of SC2, we assessed whether an ensemble method—based on an aggregation of all submitted models—could yield a better overall model, a phenomenon called “wisdom of the crowd”^{9,14}. By applying a Spectral Meta-Learner (SML)¹⁵ as our ensemble approach, we achieved a modest improvement in performance (BAC = 0.693) over the best performing individual team (BAC = 0.688), as well as an ensemble of randomly selected models (BAC = 0.63, Fig. 3d).

Leveraging biological relationships improves predictions. A common strategy among top-performing teams (DMIS, NAD,

and Y Guan) was to filter molecular features, leaving only those related to known cancer drivers for subsequent modeling (Supplementary Methods). These teams also consolidated pharmacological and/or functional pathway information associated with the molecular drug target, enabling one drug’s model to learn from data generated for another drug with the same target (Y Guan¹⁶ and NAD^{16–18}).

We took two approaches to analyze each feature type’s importance, particularly whether incorporating molecular features and chemical/biological knowledge can increase prediction accuracy. In the first approach, we generated a baseline model (following Team NAD’s method) utilizing only cell line and drug labels as input features as per SC1B. We then assessed changes in the primary metric after the substitution or addition of feature types (Fig. 4a and Supplementary Methods). In the second approach, we started with the DMIS model obtained from SC1B, and then iteratively removed single feature types and pairs of features to assess changes in prediction accuracy (Fig. 4b and Supplementary Methods).

Surprisingly, high primary metrics were observed for the NAD baseline model where the only input features were drug and cell line label (Fig. 4a, 0.32). Drug target was the only feature to improve performance of the NAD baseline model when swapped with drug label (Fig. 4a, *t*-test *P* = 0.012). Furthermore, removing both drug label and target resulted in the highest performance drop for the DMIS model (Fig. 4b, -0.17). This result highlights the importance of the global cell-line state in predicting drug synergy, and how drug target information shared across drugs can facilitate transfer learning across separate models. Mutational and copy-number variation (CNV) data can similarly offer a barcode of cell identity to encode cell line label. However, where mutation data improved performance when replacing cell line labels, replacement with CNV decreased performance significantly (Fig. 4a, *t*-test *P* = 8.8e-6). Importantly, in all cases additional feature data increased performance when added to the NAD baseline model (Fig. 4a, *t*-test *P* = 0.009, 0.009, 0.002, 0.008, 0.021 adding drug target, KEGG pathway, Gene Ontology,

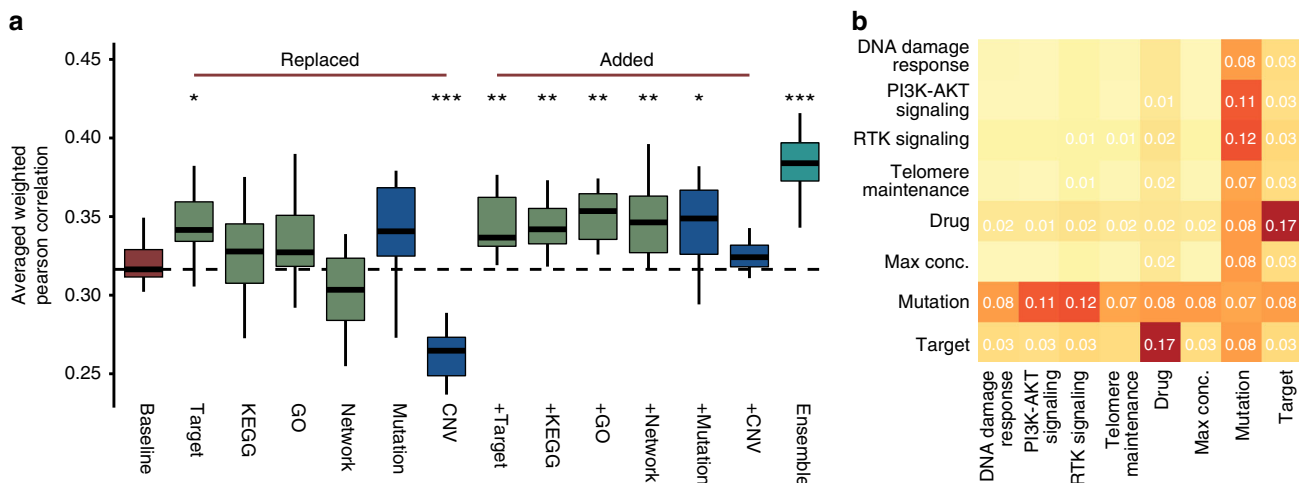


Fig. 4 Feature impact. Drug target annotation is key in top-performing algorithms, as is the meta information about variants including their functional impact and tumor driver gene status. **a** Cross validation-based distributions of NAD primary metric of SC1B when replacing or adding drug/cell line label with respective features. NAD baseline model (red) used cell line labels and drug labels only as feature inputs. In the other models different drug specific (drug targets, drug target KEGG pathway memberships, drug target-associated Gene Ontology terms or direct interactions between drug targets in a signaling network) or cell line specific (mutations or CNVs of selected, cancer related genes) features (green and blue, respectively) were added either in place of or in addition to the baseline model features. Ensemble model (cyan) is the averaged prediction of the different models. Single asterisks refers to *t*-test *P* < 0.05, double asterisks for *P* < 0.01, and triple asterisks for *P* < 0.001 compared to baseline model. **b** Heatmap of decrease in performance (average weighted Pearson correlation) of SC1B for DMIS support vector regression method when a particular feature type is removed (diagonal) or two feature types are removed at once (off diagonal)

signaling network, and mutation features, respectively). Ensemble of different feature sets improved prediction most when collectively increasing coverage of biological (pathway) complexity (Fig. 4a, t -test $P = 1.2e-6$).

Inspecting consistently poorly predicted drug combinations.

While a global performance metric applied to all cell-lines and drug combinations provides a broad assessment of model prediction accuracy, we hypothesized that some models may be optimized for certain subclasses of combinations and/or tumor types. We assessed the Pearson correlation between predicted and observed synergy scores for each combination in SC1A/B, and clustered teams by correlation of performance across combinations. Of the 118 combinations that had observed synergy scores >20 in more than one cell line, we identified 22 combinations predicted poorly by all participants (Fig. 5a, Methods), and over 50 combinations predicted well across all teams.

Combinations tested across a higher diversity of tumor types tended to show lower overall performance (Supplementary Fig. 8a; t -test $P = 0.04$), indicating that a pan-cancer prediction presents a more difficult prediction task. Combinations tested across more tumor types were also tested across greater numbers of experiments (Supplementary Fig. 8b; Spearman = 0.56,

$P = 2.3e-15$), but no significant difference was observed between performance and number of experiments within a cancer type specific setting (Supplementary Fig. 8c, d). On average the quality assessment scores were significantly better (t -test $P = 0.018$) for the pharmacology experiments in the training set of well predicted compared to poorly predicted combinations (Supplementary Fig. 8e). Comparable trends were seen between the quality of synergy and predictive performance in the training and test sets (Supplementary Fig. 8f; $r = 0.52$ vs. 0.43). The distribution of synergy scores were similar between poorly and well predicted combinations (Supplementary Fig. 8g) as were the proportion of synergistic cases (37% for poorly predicted vs. 39% for well predicted).

Well predicted cases were enriched for combinations inhibiting both the PI3K/AKT and MAPK pathways (Fig. 5b, average Pearson $r = 0.37$ vs. 0.25; t -test $P = 0.008$), or apoptosis pathway combined with either metabolism, cell cycle, or receptor tyrosine kinase pathways. The drugs targeting these pathways were prevalent in our dataset, but these specific combinations of those drugs were not (Supplementary Fig. 9a). Assessment of the interactions between drug targets and neighboring proteins from *OmniPath*, a comprehensive compendium of literature-based pathway resources¹⁹, revealed no differences in the somatic alteration frequency for targets or their first neighbors between

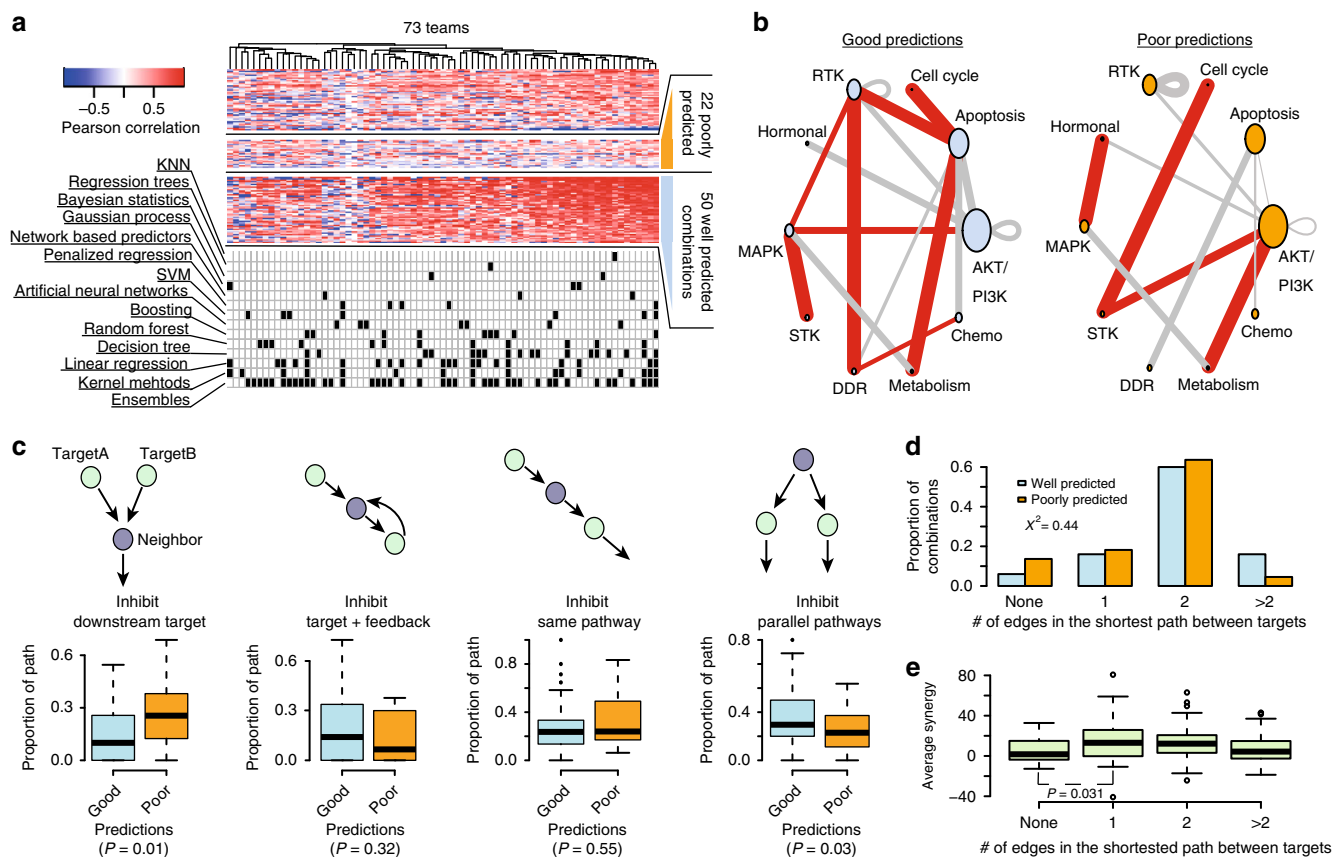


Fig. 5 Features of poorly and well predicted combinations. **a** Heatmap of Pearson correlation between observed and predicted synergy scores for 118 combinations across 73 teams participating in SC1A/B. Algorithms used by each team is marked in the matrix below. **b** Combinations of pathways targeted. Size of node is proportional to number of drugs targeting a specific pathway in the entire dataset and width of edges is proportional to the number of drug combinations within the poorly or well predicted combination subset. Red edges highlight target pathway combinations unique to either the well predicted or poorly predicted combinations. **c** Types of interactions between the nearest neighboring gene and the two drug targets of poorly and well predicted combinations. Boxplots show the difference in the proportion of interactions of each type for poorly and well predicted combinations (t -test). **d** Proportion of poorly and well predicted combinations for different network distances (minimum number of interactions in the *OmniPath* shortest path) between the two targets of a drug combination, difference significance estimated with chi-squared test. **e** Difference in average synergy for combinations categorized by the network distance between targets are tested with t -test

the poorly and well predicted combinations (Supplementary Fig. 9b, c). We did observe a significant enrichment of well predicted combinations where both drugs' respective targets were downstream of a common neighboring protein (Fig. 5c, t -test $P=0.01$), and conversely, we observed an enrichment of poorly predicted combinations where targets were both up-stream (Fig. 5c, t -test $P=0.03$). There was no significant difference (Chi-sqr $P=0.44$) in OmniPath protein network distance between drug targets for well and poorly predicted combinations (Fig. 5d), nor any correlation between either network distance and average/median synergy scores (Fig. 5e) or the number of cases with synergy >20 . Combinations where targets were found to not be connected in a protein network had significantly lower average synergy (t -test $P=0.031$) and lower max synergy (t -test $P=0.0021$).

Biomarkers of drug combination synergies. A limitation of many machine learning algorithms is the lack of feature interpretability and experimentally testable logic-based rules. We took two approaches to identify biomarkers that may be predictive of drug synergies: a direct survey of participants through which predictive features were nominated for each drug pair (Supplementary Data 2); and retrospective work focusing on results from two of the best performing teams, NAD and DMIS, to deconvolute features most impactful to model predictions (Supplementary Fig. 10 and Supplementary Data 3).

The survey-submitted biomarker results varied in detail and depth (Supplementary Data 2), but common genetic markers were apparent across good predictions in SC1B, including *EGFR*, *ERBB2*, *PIK3CA*, *PTEN*, *TP53*, or *RB1*. In the survey, synergy was commonly assigned to drug pairs targeting directly down- or up-stream of a mutated, amplified, overexpressed or deleted cancer gene. We hypothesized that drug synergy may result when one drug overcomes a resistance mechanism for the other. Focusing on mutations in cancer genes (as defined by Iorio et al.¹²) we identified all mutations associated with resistance to monotherapy in our data (Supplementary Methods and Methods) selected at increasingly stringent P -value (wilcoxon rank sum test) thresholds (Supplementary Methods and Methods). For each threshold, we then assessed the likelihood of synergy seen from combinations paired to these monotherapies in the presence vs. absence of the respective mutation. We observed an increase in the proportion of synergistic drug combinations with each increase in threshold stringency (Fig. 6a, Pearson $r=-0.90$, $P=4.09e-38$). We observed the same trend in patient-derived xenograft (PDX) models (Fig. 6b, Pearson $r=-0.95$, $P=2.2e-49$). This observation supports the notion that drug sensitivity may be restored with drug combinations targeting a resistance driver.

We also explored models of best performing teams and their chosen features, focusing on biomarker associations aligned to combinations for which the respective team had achieved a robust prediction accuracy (Pearson $r>0.5$), with particular interest in the genetic biomarkers revealed through SC1B. Multiple criteria for quality, independence and reproducibility (Methods)^{4,8} were applied yielding 13 feature-to-combination associations (Fig. 7a and Supplementary Data 3), seven associated with synergy and six with non-synergy. To assess whether these associations could be independently validated as synergistic biomarkers, we explored nine overlapping and 21 non-overlapping (independent) cell lines in O'Neil et al.⁴ (Fig. 7b) that were treated with similar drug combinations, i.e., same putative drug targets. Concordance of association was observed in the nine overlapping cell lines (Fig. 7c; six out of seven associations, ~86%) and in the 21 independent cell lines (Fig. 7d; eight out of eleven associations, ~72%).

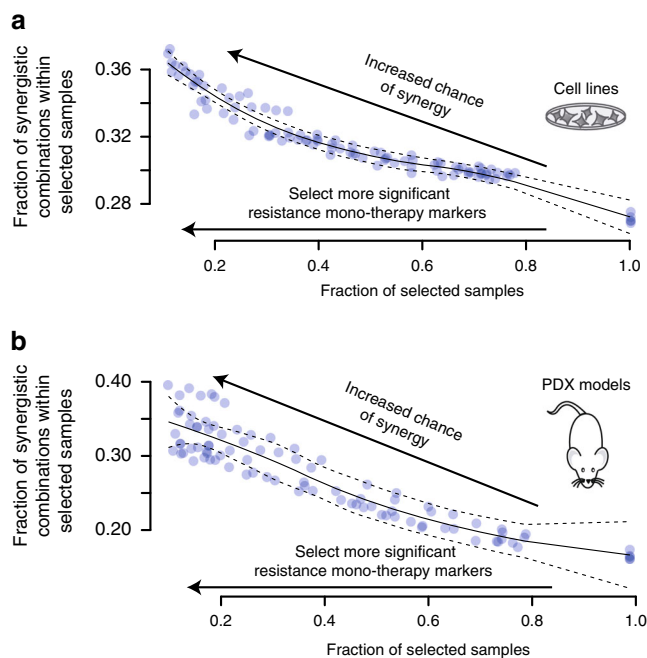


Fig. 6 Drug synergy and monotherapy resistance biomarker relationship. **a** Cell lines and **b** PDX models show increased frequency of synergistic drug combinations if they contain biomarkers with stronger association to monotherapy resistance (Methods; Supplementary Methods). The fraction of combination experiments is selected by order of most significant linked monotherapy resistance biomarker associations. The solid and dashed line are the LOcal regrESSion (LOESS) curve fit and its standard error, respectively

Among the prioritized feature-to-combination associations were several genetic variants associated with synergistic responses to the combination of receptor tyrosine kinase (RTK) inhibitors with inhibitors of the downstream PI3K/AKT pathway. Amplifications or activating mutations in *EGFR* or *ERBB2* consistently predicted synergy from inhibition of the RTK + PI3K/AKT pathways across multiple independent drugs and datasets (Fig. 7a). Less direct relationships were also observed, including combined AKT inhibition with either IGFR inhibition in the *ERBB2* mutant setting or FGFR inhibition in the *EGFR* mutant setting (Supplementary Data 3). Despite kinase domain homology it is unlikely these observations are explained by off-target effects since *EGFR*, *ERBB2*, and *FGFR* mutations were only predictive of respective monotherapy responses (Supplementary Fig. 11). Combinations inhibiting multiple points within the PI3K/AKT pathway also showed synergy in the presence of up-stream activation from mutations in *PIK3CA* or deleterious events in *PTEN* (Fig. 7a, e). Inhibition of the metalloproteinase ADAM17, known to influence RTK activity²⁰, also showed synergistic responses in a common subset of cell lines when combined with inhibitors of PIK3C-pan or AKT1/2 (Fig. 7a and Supplementary Data 3), with a notable exception of PIK3CB/D selective inhibitors, which show antagonism unique to *PIK3CA* mutant cell lines (Fig. 7e, f). Amplification and activating mutations in Androgen Receptor (*AR*) were also found to be associated with antagonistic effects when targeting AKT in combination with MAP2K or IGFR inhibitors (Fig. 7a).

Translatability of synergy and biomarker predictions. We assessed the performance of top-performing AstraZeneca-DREAM models on the independent screening datasets by O'Neil et al.⁴ and ALMANAC¹³. Since no combination-cell experiments

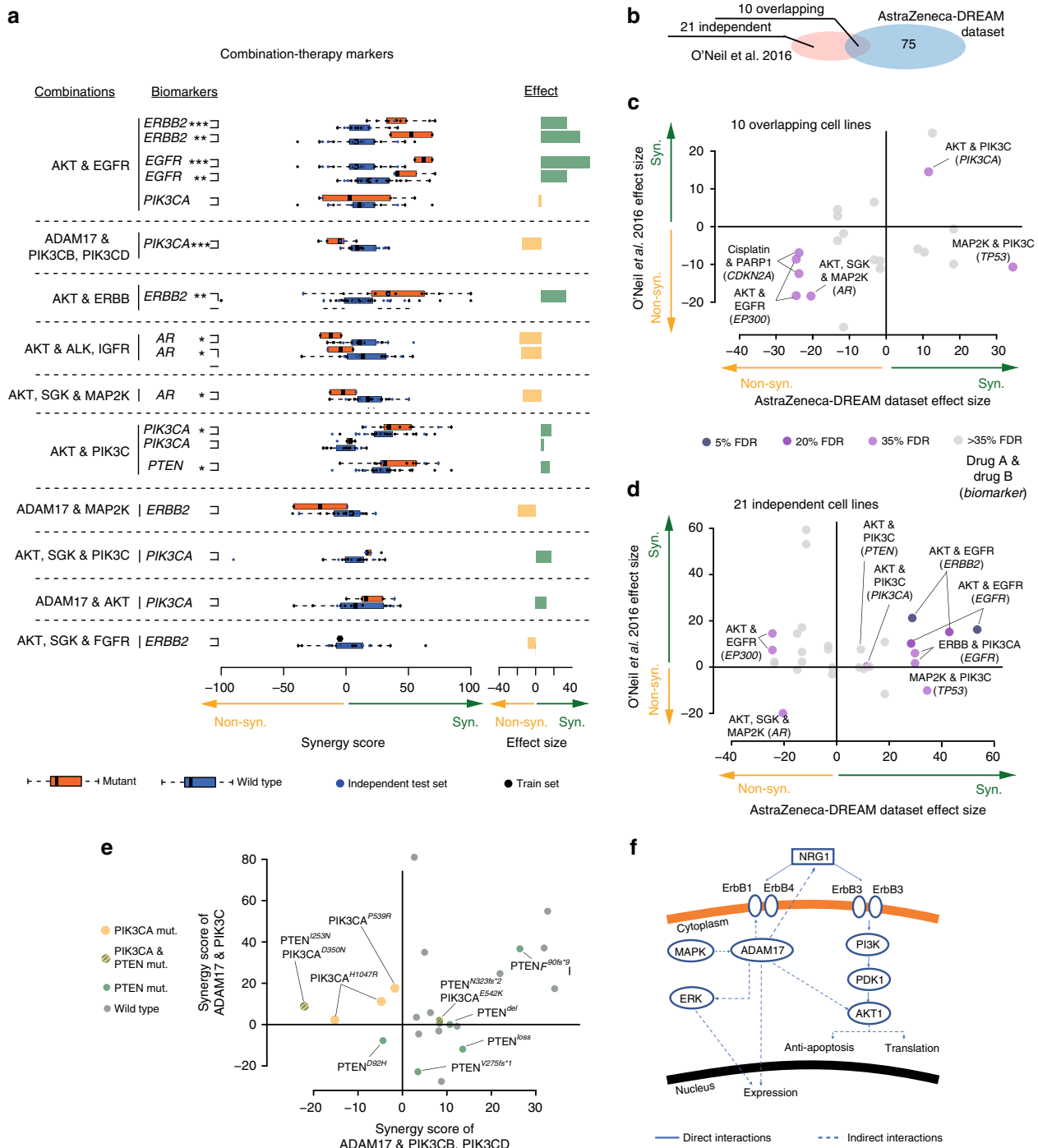


Fig. 7 Post-hoc analysis of putative synergy biomarkers. **a** Synergy markers suggested by DMIS and NAD, when focusing on top weighted features from predictive models filtered for biological relatedness to drug targets, ANOVA with FDR of triple asterisks refers to 5%, double asterisks refers to 20% and single asterisks to 35%. **b** Venn-diagram showing independent and overlapping cell lines between AZ-DREAM and O'Neil et al.⁴. Independent dataset reproducibility of biomarker predictions in **c** the overlapping and **d** O'Neil et al.⁴ exclusive cell lines. The effect size is the mean difference in synergy scores of mutant vs. wild-type cell lines. **e** Comparison of ADAM17 combined with PIK3CB/D against ADAM17 in combination with pan-PIK3C inhibitor. **f** Network cartoon of PI3K signaling and role of ADAM17

directly overlapped AZ-DREAM and O'Neil et al.⁴, we collapsed drugs by shared targets to expand the overlap. We observed that SC1A models from NAD and DMIS outperformed random models (Fig. 8a, mean primary metric = 0.07, top 1% of random models) for cell lines and drug target combinations non-overlapping between O'Neill et al. and AZ-DREAM data (Supplementary Data 1). Interestingly, no substantial performance increase was observed when independent model predictions were

made for the ten cell lines in common between the two datasets, nor the 30 combinations with similar chemical/target properties (Supplementary Table 2 and Fig. 8b-d). As in the main Challenge, combining these two or more models in an ensemble led to an improved prediction performance (Fig. 8a-d).

Considering the limited overlap and correlation of synergies between AZ-DREAM and ALMANAC datasets, high performance was not expected when predicting ALMANAC synergy

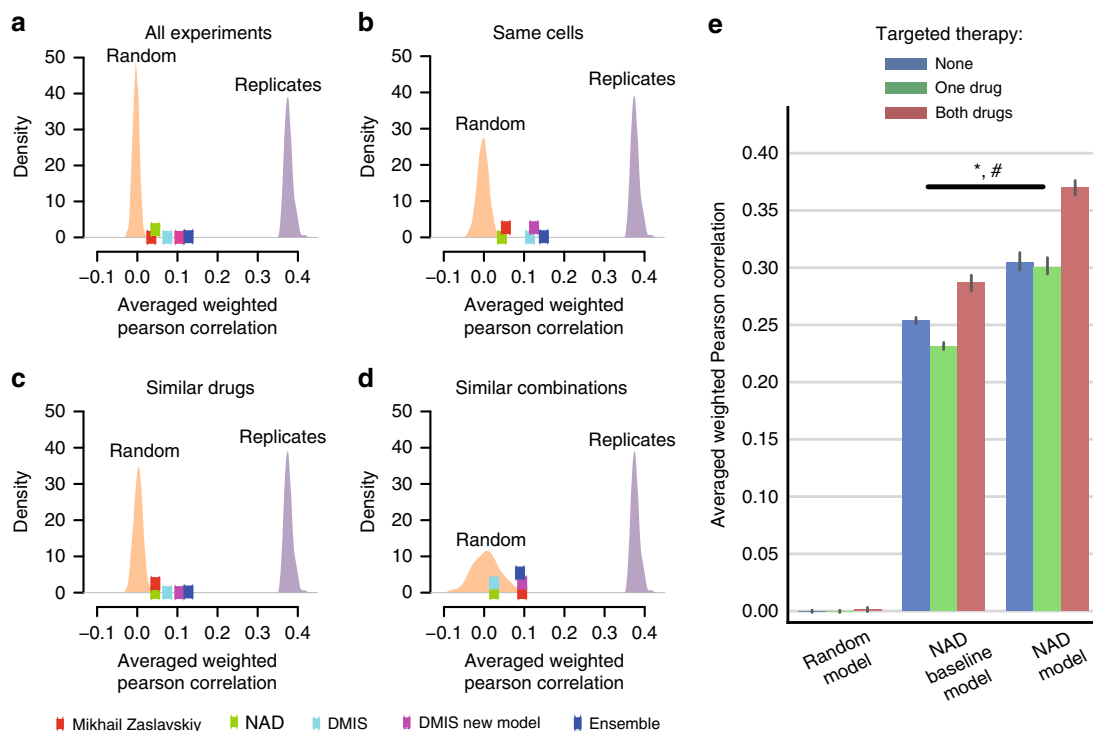


Fig. 8 Translatability of AstraZeneca-DREAM models to the independent screens. Performance of SC1A models for predicting synergy scores in the O’Neil et al.⁴ dataset by the best performing teams are plotted along with distributions of predictions from the random model and replicate experiments. Performance of predictions are shown for **a** all experiments in the O’Neil et al.⁴ dataset, and three subsets of the dataset; **b** experiments that tested same cell lines as AZ-DREAM, **c** tested similar drugs as in AZ-DREAM (one drug in the combination with the same target), and **d** tested similar combinations as in AZ-DREAM (same targets for both drugs in the combination). **e** Prediction performance on the ALMANAC¹³ dataset is shown for a random, NAD baseline (using only cell line and drug identities as features) and full NAD model for no targeted agents (None, i.e., two chemotherapeutic drugs), one targeted agent plus chemo (One drug), and combinations of two targeted agents (Both drugs)(mean \pm 95% CI). ANOVA *P*-values: **P* = 1.322e-31 for different performance between baseline and full model; #*P* = 5.584e-5 for association between model performance and number of targeted drugs in the combinations

scores with models trained on AZ-DREAM data points alone, as was observed for the NAD model. We trained two NAD models on 50% of the ALMANAC data: first a baseline model to show maximum performance achievable when using only cell and drug label features as input; and a second allowing use of the full feature set as input. The full model consistently predicted significantly better than baseline in the remaining 50% over ten randomized iterations, giving confidence in the transferability of the method designed for AZ-DREAM. Best performance was observed for targeted combinations ($r = 0.369$ vs. 0.287 for full NAD and baseline NAD model, ANOVA *P* = 1.322e-31 for model type and *P* = 5.5e-05 for model type and targeted therapy association, Fig. 8e).

Exploring AZ-DREAM biomarker associations prioritized as described in earlier sections, we assessed statistical association for drug combinations with consistent targets in the O’Neil et al.⁴ dataset. In the ten cell lines overlapping the AZ-DREAM and O’Neil et al.⁴ datasets, seven of the prioritized biomarker-drug combinations were present, of which six (86%) showed reproducible directionality (FDR < 35%, Fig. 7c). In the 21 O’Neil et al.⁴ cell lines not used within AZ-DREAM training, 11 of the prioritized biomarker-drug combinations were present, of which 8 (72%) showed reproducible directionality (Fig. 7d).

Discussion

The objective of this AstraZeneca-DREAM Challenge was to drive the development of innovative computational approaches to predict novel drug combinations and to comprehensively

benchmark these approaches. To enable this we made one of the largest in vitro drug combinatorial screens to date available to the scientific community. We cover largely non-overlapping experiments to existing datasets and, in particular, offer extensive data for targeted therapies complementing the non-targeted chemotherapeutic agents covered in the NCI-ALMANAC. Despite little overlap we demonstrated an encouraging reproducibility of data and predictions between screens, particularly when considering the confounding differences in experimental designs and assay formats²¹. Furthermore, we showed that some trends represented in these data can be reproduced in vivo, and that clinically efficacious combination pairs can be identified. Our double-blinded benchmark of 78 methods provides an unbiased comprehensive evaluation of the state-of-art of drug synergy prediction. Collectively this Challenge manuscript equips the scientific community with data and a methodological baseline for algorithm development, alongside a suite of computational methods to direct new experiments towards likely synergistic drug combinations.

The results of the AstraZeneca-Sanger Drug Combination Prediction DREAM Challenge have shed important light on the best practices and limitations in predicting drug synergy. By evaluating predictions from a large number of teams, we were able to discern important strategies for predicting drug synergy from molecular and chemical traits. As with most DREAM Challenges, we observed that the machine learning method itself has little impact on overall performance. Aggressive pre-filtering that incorporates clean sparse network data to consider feature relevance to drug targets and cancer was successfully used by top

performers to limit model complexity and improve model generalizability. Despite the complexity of the problem, many teams reached the upper-bound of performance levels based on variability in experimental replicates. This was further confirmed when top-performing models were applied to an independent dataset, demonstrating robustness to assay variability, and context heterogeneity.

A comprehensive assessment of the predictive value of monotherapy was not completed in the Challenge format, in part due to initial miss-annotation of data. However, post-hoc analyses suggested it offered no significant improvement to well-performing models (Supplementary Fig. 12). Despite minimal predictivity from monotherapy itself as a feature, biomarkers associated with monotherapy resistance were observed to have predictive value for respective combinations. Looking forward, additional attention is also required for the one-fifth of combinations poorly predicted by all Challenge teams. The rationale differentiating these combinations is non-obvious but our data suggests, in part, some relationship to the complexity of network connectivity between drug targets and proximal biomarkers (Fig. 5c), perhaps a bias introduced by network-led dimension reduction techniques employed by well-performing models. Furthermore higher synergy scores were observed—in some combinations—when both drugs target downstream of a commonly interacting protein²². Collectively, these observations advocate for a more biologically rationalized approach to biomarker discovery, accounting for directionality and exclusivity of signaling and functional relationships between biomarkers and targets.

A notable absence from the Challenge was the use of mathematical, reaction- or logic-based mechanistic pathway modeling approaches^{23–27}, likely due to the higher time and data input needed for model creation. The dynamic nature of mechanistic models may offer an advantage by enabling consideration of the heterogeneity that exists across even apparently ‘clonal’ cell line populations²⁸. The increasing availability of published pre-derived mechanistic models for many cancer relevant pathways may soon make such an approach more viable. Given the strong benefit seen from inclusion of prior-knowledge, and as text-based artificial intelligence technology matures, computational approaches, such as natural language processing (NLP) to harness knowledge from world literature may also become of significant benefit. Alternatively, more generic signatures of dynamic (e.g., transcriptional) output may first be used to identify a mechanistic rationale^{28–31} to which causative genetic or epigenetic events can then be inferred and aligned as predictive features^{32,33}. A surprising result of our Challenge, however, suggested only modest improvement to prediction from inclusion of all data in SC1A compared to only genetics in SC1B.

To maximize potential for translation it is essential that modeling approaches reveal testable biological insight, particularly considering that this and prior Challenges show no predictive advantage to black box algorithms. As we discovered, however, it can be difficult to incentivize knowledge retrieval within a competition format that focuses on objective scoring of performance. Despite these limitations, we were able to extract important insights to biomarkers for certain drug combinations. Given the dominance of RTK and PI3K/AKT pathway targeting agents in the Challenge data, it was not surprising that these revealed some of our strongest combination-feature relationships. In multiple cases this aligned to a two-hit hypothesis targeting the activating driver with a downstream pathway component. These included synergies between EGFR and AKT inhibitors in the presence of activating *EGFR* mutations³⁴, or AKT1/2 with pan-PI3K inhibitors in the presence of pathway activating mutations

in *PIK3CA* or *PTEN*. In some cases the biomarker rationale for AKT inhibitor synergy with RTK or MAPK inhibition was less direct but indicative of crosstalk and feedback signaling previously reported³⁵. Interestingly antagonism was observed in cell lines harboring activating mutations of *AR*^{36–39}. Feedback signaling resulting from AKT inhibition has been seen to drive AR activity, which in turn can lead to the activation of the MAPK cascade^{39,40}, attenuating respectively targeting drug activity.

The synergy observed between ADAM17 and PI3K/AKT pathway inhibitors may work through independent inhibition of multiple cancer hallmarks, or via a more direct mechanism whereby inhibition of ADAM17 driven proteolysis and shedding of RTKs²⁰ stabilizes and increases signaling through PI3K/AKT^{41,42}. Notably ADAM17 predominantly influences RTKs other than EGFR/ERBB2²⁰, and no benefit is seen in cells with mutations in these genes. ADAM17 inhibition, however, showed antagonism unique to combined PI3K/D selective inhibitors within the *PIK3CA* mutant setting. Reduced synergy may result from a lessened dependency on PI3K paralogues in the presence of constitutively activated *PIK3CA*, or reduced benefit from ADAM17 loss in the extreme luminal/epithelial physiology of *PIK3CA* mutants. The apparent antagonism, however, suggests feedback following PI3K/D inhibition enhances mutant *PIK3CA* expression/activity. Indeed PI3K/D inhibition has been shown to result in elevated expression and activity of *PIK3CA*⁴³, and may also relieve the inhibitory effects of substrate competition or dimerization between *PIK3CA* and *PIK3CB/D*.

Many drug combinations effective in the clinic to date involve mechanistically distinct agents, often chemotherapies combined with an additional targeted therapy, for which benefit may arise from the independent effects of the drugs on different sub-populations⁴⁴ rather than synergy. More recently, an increasing number of combinations include multiple targeted therapies⁵. Hence, identifying both molecularly synergistic and complementary drugs, and how these affect inter- and intra-patient heterogeneity remains an essential area of future research. Future Challenges should further address the question of how to optimize translation of preclinical results into the clinic⁴⁵. Where this Challenge addressed prediction of synergy for combinations of known drugs, an ability to predict truly novel beneficial target combinations should also be explored. Furthermore, the space of therapeutic combinations should be extended to include >2 drugs, and covering targets in independent cell types, such as subclonal tumor cell populations or cells of the tumor microenvironment and immune system³. These approaches can be complemented by adaptive and sequential strategies reactive to monitoring of the patient tumor and physiology. Success in these areas will be dependent on the availability and access to large-scale data needed for model development and validation. Public-private partnerships—as exemplified by this Challenge and AstraZeneca’s generous sharing of data with the research community—will be critical to future efforts.

Methods

Drug combination screening. All cell lines were authenticated at AstraZeneca cell banking using DNA fingerprinting short-tandem repeat assays and each bank is confirmed to be free from mycoplasma. Cells ordered from the global cell bank are cultured for up to 20 passages. Cell suspensions are counted using a haemocytometer and cells are re-suspended in full growth medium containing Pen/Strep to a final density for different cell line densities and for different seeding densities into 384-well cell culture plate. A volume of cells as determined by cell count and dependent on cell type was added to each well of a Greiner 384-well plate using a Multidrop Combi liquid handler and then incubated at 37 °C and 5% CO₂ overnight in a rotating incubator. After seeding, plates were shaken to distribute the cells more evenly at the bottom of the wells and left to stand on the bench for 1 h to allow even settling of cells.

Drug combinations were screened with four combinations per 384-well plate in a 6-by-6 range of concentration format. The first row and first column in the 6-by-6 matrix are monotherapies of each drug in the combination, while the top left corner is the untreated control. Drug combinations therefore were tested in a 5-by-5 layout with comprehensively rescreening the monotherapy and control for each experiment to minimize batch effects. Drug concentrations ran from the highest dose to the lowest dose. All plates were dosed with drugs solubilized in DMSO or PBS, or DMSO alone to provide comparable treatment and max control wells. After 5 days of incubation 5 μ l of 2 μ M Sytox Green working solution was added to each well of the 384-well plates (0.133 μ M final concentration) and the plates incubated for 1 h at room temperature. After incubation plates were read by the Acumen laser scanner to detect the number of Sytox Green stained cells. The total fluorescent intensity across the well was then read and the number of dead cells calculated by dividing this total fluorescence by the fluorescence of a single cell. The plates were re-read on the Acumen to give a total cell count. A live cell count was then determined by subtracting the dead cell count from the total cell count.

Quantifying combination synergy and antagonism. Synergy and antagonism were quantified in an automated way using freely available Combeneft software (v1.31)¹¹. The approach implemented in Combeneft is based on quantifying synergy distribution by comparing a drugs combination experimental dose-response surface to a modeled reference based on individual drugs dose-response curves. Briefly, for each 6-by-6 matrix, monotherapy dose-responses were extracted and modeled as a sigmoidal curve via the Hill equation⁴⁶. A reference dose-response surface is then generated by Combeneft based on the Loewe model of additive combinations and the single drug dose-response curves. The experimental combination dose-response surface is then compared by the software to the model-generated one, resulting in a synergy distribution in concentration space. This synergy distribution is finally further summarized by integrating the synergy distribution in logarithmic concentration space. The procedure resulted in a single score (the result of this integration) for each combination.

In vivo response class definitions. Response data for 62 treatments across ~1000 PDX models were derived from Gao et al.⁸ Putative drug targets from the AZ-DREAM and Gao et al.^{4,8} dataset were utilized to identify overlap. As synergy scores were not available for the Gao et al.^{4,8} dataset, “Best Response” (complete response-CR, partial response-PR, stable disease-SD, progressive disease-PD) for each combination-PDX pair were extracted and compared with monotherapy “Best Response” of each drug in the combination on the same PDX model. This was represented numerically where CR = 4, PR = 3, SD = 2, and PD = 1. Synergy was assigned to a change of +2 or more, and Antagonism to a change of -2 or less. A change of +1, 0, or -1 was assigned Additive, considering an element of experimental variability. Cases where best response has been observed as a range over time (PR \rightarrow PD), the earliest response was considered as we hypothesize this to reflect in vitro response in a more realistic sense for comparison.

The percent tumor volume change class definitions are as following:

1. Synergistic efficacy: Combination treatment leads to better tumor regression than either monotherapy.
2. Synergistic non-efficacy: Combination response is better than either monotherapy but does not result in tumor regression.
3. Additivity: Combination response same as the better of either monotherapy responses.
4. Non-synergistic efficacy: Combination response weaker than the better of the monotherapy responses but results in tumor regression.
5. Antagonism: Combination response weaker than both monotherapies.

In vitro response class definitions. Response scores defined by the Loewe synergy model were considered in ordered to define in vitro response classes. Synergism was defined as Loewe scores ≥ 20 , Antagonism ≤ -20 , and rest are classed as Additive.

Molecular characterization. The 85 cell lines were molecularly characterized, including:

1. Mutations from whole exome sequencing with Illumina HiSeq 2000 Agilent SureSelect (EGAS00001000978)
2. Copy-number variants from Affymetrix SNP6.0 microarrays (EGAS00001000978)
3. Gene expression from Affymetrix Human Genome U219 array plates (E-MTAB-3610)
4. DNA methylation from Infinium HumanMethylation450 v1.2 BeadChip (GSE68379)

Mutations were called with CAVEMAN [<https://github.com/cancerit/CAVEMAN/>]⁴⁷ and PINDEL [<http://gmt.genome.wustl.edu/packages/pindel/>]⁴⁸ as reported in ref. ¹². Variants were provided without further filtering, including putative passenger mutations, germline variants, and potential cell line artefacts, which are in total 75,281 mutations in 85 cell lines.

Copy-number variants (CNVs) are called with the PICNIC [<http://www.sanger.ac.uk/resources/software/picnic/>]⁴⁹ algorithm using the human genome build 38 as the reference. CNVs might be wild type, deletion, or amplification of certain segments in a chromosome. One or multiple genes can fall within such segments. We reported copy number for the major and minor allele on gene and segment level.

Gene expression was processed as described in ref. ¹², including Robust Multi-array Average (RMA) normalization with the R-package ‘affy’⁵⁰. Gene expression for 83 cell lines across 17,419 genes (HGNC labels) was reported; no expression was available for MDA-MB-175-VII and NCI-H1437.

DNA methylation was reported for 82 cell lines the *beta* and *M* values⁵¹ for 287,450 probes; no methylation was available for the cell lines SW620, KMS-11, and MDA-MB-175-VII. In an additional processing step, CpG sites were compressed to CpG island with the definition from UCSC genome browser⁵², resulting in a total of 26,313 CpG island based on either *M* or *beta* values.

Drug properties. The identity of all drugs was anonymized, but for all agents the putative targets are revealed. The gene names of the protein targets are listed with “*” denoting any character if the target is a protein family. Furthermore, for 58 drugs the Molecular weight, H-bond acceptors, H-bond donors, calculated octanol-water partition coefficient, Lipinski’s rule of 5, and their SMILES (Simplified Molecular Input Line Entry Specification) are provided. Drugs were grouped into pathways and biological processes manually according to their protein targets (Supplementary Data 1).

Challenge organization. The Challenge consisted of two sub-challenges, each with multiple rounds: a leaderboard, validation, bonus, and collaborative round. SC1 had four leaderboard rounds that lasted 8, 6, 5, and 5 weeks, while SC2 had three leaderboard rounds that lasted 12, 7, and 5 weeks. Participants were given a leaderboard dataset to build a model and generate three prediction files per leaderboard round. Scores were returned to participants so that they can improve their model throughout these rounds for their one submission to the final round, which was scored against a held-out dataset. The final round lasted for 2 weeks, which was then followed by a 9 week bonus round and 10 week collaborative round.

Challenge pharmacology data splits. In SC1, participants were asked to predict drug synergy of 167 combinations in the panel of 85 cell lines. The synergy data of each drug combination was partitioned into three sets: a training dataset (3/6–50%), a leaderboard set (1/6–16.7%), and validation set (2/6–33%) of treated cell lines. SC2 leveraged data for remaining 740 drug combinations not overlapping with those used in SC1, although data for some of the same drugs (in combination with different drugs), homologous drugs (i.e., same target, but different chemical structure), and cell lines were included. A leaderboard set (370 combinations) and a final validation set (370 combinations) were randomly split, which are mutually exclusive from each other, as well as from SC1.

Primary scoring metric of Sub-Challenge 1. With synergy scores roughly normally distributed and outliers truncated to -100 and 100 (Supplementary Fig. 2), Pearson’s correlation was employed as the base measure of prediction accuracy within each drug combination. The primary metric was then the average weighted Pearson correlation (ρ_w) of the predicted vs. observed synergy scores across each individual drug combination, *i*. The weight for a given drug combination *i* was $\sqrt{n_i - 1}$ where n_i is the number of cell lines treated with the drug combination. This resulted in the following primary metric for SC1A&B,

$$\rho_w = \frac{\sum_{i=1}^N \sqrt{n_i - 1} \rho_i}{\sum_{i=1}^N \sqrt{n_i - 1}}, \quad (1)$$

where $N = 167$ were the tested drug combinations.

Tie-breaking scoring metric of Sub-Challenge 1. The tie-breaking metric was identical to the primary metric Eq. 1 except that it was applied to the subset of drug combinations that have at least one cell line with synergy score $S_{ci} \geq 20$ in the held-out test set (S_{ci} = synergy score at cell line *c* and drug combination *i*). Neither the subset of drug combinations nor its size ($N = 118$) was revealed to participants prior to final evaluation.

Primary scoring metric of Sub-Challenge 2. The primary metric was a sequential three-way ANOVA, which tested the separation of held-out synergy scores by predicted synergy (=1) and predicted non-synergy (=0). In the sequential three-way ANOVA (type 1), we controlled for systematic drug and cell line effects, and evaluated variance explained by a given team’s synergy predictions. We define the primary metric as

$$SA = -\text{sgn} \times \log_{10}(p), \quad (2)$$

where *sgn* is the sign of the effect size (positive or negative separation by prediction), and *p* is the *P*-value (*F*-statistic) computed from the ANOVA distinguishing predicted synergy (=1) from predicted non-synergy (=0) across all experimentally measured synergy scores.

This three-way ANOVA score can be interpreted via linear regression where the intercept is set to 0.

$$y \sim \beta_1 \cdot dc + \beta_2 \cdot cl + \beta_3 \cdot x \quad (3)$$

Here, the response variable y is the observed synergy, which is normally distributed, and there are three predictive features: dc = drug combination, cl = cell line and x are synergy predictions. Then the primary metric, $SA = -\log_{10}(p.value[\beta_3]) \cdot xsign(\beta_3)$, measures the significance of a team's predictions after controlling for variance associated with cell line and drug combinations.

Tie-breaking scoring metric of Sub-Challenge 2. As the tie-breaking metric, we used balanced accuracy (BAC) using discretized synergy scores $S_{ci} \geq 20$ to evaluate the binary classifiers submitted in this sub-challenge. This metric evaluates both the sensitivity and specificity of the classifiers while taking into account the low proportion of synergistic cases to un-synergistic.

Application of the Tie-Breaking Metric. In each sub-challenge, we estimated a Bayes Factor (BF) using a paired bootstrapped approach to determine whether a team's score was statistically indistinguishable from another. In the event that a team's scores were determined to be statistically equivalent, we then applied the tie-breaking metric. To estimate the BF, we sample with replacement from the M observations of the given sub-challenge and computing the primary metric (pm) for each team 1000 times. For a given team, T , K_T was computed by

$$K_T = \frac{\sum_{i=1}^{1000} pm_{T,i} < pm_{best,i}}{\sum_{i=1}^{1000} pm_{T,i} \geq pm_{best,i}} \quad (4)$$

Where $pm_{best,i}$ is the bootstrapped primary metric at iteration i for the team with the highest primary metric (non-bootstrapped).

Assessing performance of individual combinations. Combinations defined as poorly predicted had an average predicted vs. observed Pearson correlation across teams in the range seen with a random predictor (SC1 Primary metric = -0.25 and 0.25). In contrast, well predicted combinations had an average Pearson correlation across teams of above 0.5 .

Independent validation on O'Neil et al. Merck screen. In order to assess the utility of features and the predictability of the learning algorithms in new contexts, we provided the participants an independent large-scale oncology combination screen published recently⁴. The O'Neil et al.⁴ dataset consists of 22,737 experimental endpoints covering 583 doublet combinations across 39 diverse cancer cell lines. Thirty-eight experimental drugs and approved drugs were included in this combination screen using a 4-by-4 dosing regimen. Raw cell viability measures for each combination experiment were processed through Combeneff¹¹ to generate synergy scores as per the Challenge dataset. While there are 6 approved drugs, 49 targets, and 10 cell lines in common between the Challenge and O'Neil et al.⁴ datasets, the total number of exact experiments (Drug A–Drug B–Cell line) overlapping is below 100, giving the participants a highly independent validation set for their prediction algorithms. This information was provided to best performing teams in the Challenge, along with a dictionary of curated chemical structures and putative targets for each. Prediction models were trained on the released Challenge dataset and made synergy score predictions on the O'Neil et al. dataset. Metrics for SC1 and SC2 were used to assess prediction performance.

Individual prediction models. Full description and implementation of models used by teams in the final submission to DREAM can be downloaded from:

[Synapse.org/AstraZeneca_Sanger_Drug_Combination_Challenge_Leaderboards](https://synapse.org/AstraZeneca_Sanger_Drug_Combination_Challenge_Leaderboards) [http://www.synapse.org/AstraZeneca_Sanger_Drug_Combination_Challenge_Leaderboards]. Top-performing prediction models in SC1 and SC2 made use of genetic features relating to the gene targets of the drugs. Feature selection from the models enabled nomination of putative biomarkers for drug combination synergy (Supplementary Methods).

Ensemble models. SC2 participant models were aggregated using two types of ensemble models Spectral Meta-Learner (SML) and Random Aggregation. SML chooses predictions from n methods to aggregate based on an estimation of BAC for each method without using actual labels^{15,53}. Random Aggregation is the traditional way that people aggregate models by giving equal weight to each method. We randomly pick n methods (do this ten times) and for n methods we compute the average BAC and the error.

Monotherapy biomarkers and synergy enrichment. Monotherapy markers are the mutational status of genes, either mutated or copy number altered, from the pan-cancer binary event matrix (BEM)¹², which separate the monotherapy response into sensitive vs. non-response. The likelihood of separation was estimated with a Wilcoxon Rank Sum test (Supplementary Methods). From most

significant monotherapy marker to lowest in 0.1 steps of $-\log_{10}(P\text{-value})$, we accumulative evaluated the percentage of synergistic combinations (synergy score ≥ 20) with at least one monotherapy marker. This analysis was bootstrapped five times with 80% of the pharmacology data (Supplementary Methods).

Synergy biomarkers. A short list of putative synergy biomarkers were derived from the five highest ranked features of well predicted drug combinations (Pearson $r > 0.5$) from the two best performers NAD and DMIS. Features were ranked based on their feature weight or importance for given well predicting model. This gene-to-combination short list, was filtered for associations predicted by both teams, or genes biological related to the drug target defined as either the gene being the target itself, a short distance to it in OmniPath signaling network (two molecules up- or downstream) or GO term similarity⁵⁴ larger than 0.7. This resulted in a list of 47 gene-to-combination associations that we further studied. A gene within this list is considered mutant if it was deleted, amplified (>7 copies) or mutated in any sense, resulting in an extended BEM¹². We calculated the P -value for each suggested association with an ANOVA correcting for tissue of origin and multiple hypothesis testing via Benjamini Hochberg. The effect sizes is the mean difference in synergy score between mutant and wild-type cell lines.

For external validation of those putative biomarkers of synergy, we focused on drug combinations in O'Neil et al.⁴, ALMANAC¹³, and additional experimental data from AstraZeneca (Supplementary Data 3). We validated biomarkers in two different contexts, (i) for cell lines overlapping with AZ-DREAM, considered as biological replicates, and (ii) cells non-overlapping for predictions on independent cell lines.

Literature evidence for the shortlisted combination-biomarker associations was identified through PubMed search. The aim was to identify published evidence of (i) the combination-biomarker association, (ii) the combination but not the specific biomarker, and (iii) either one of the targets and the biomarker association. The publications were further categorized into in vitro, in vivo, and preclinical studies. Publications that discuss the specific combination-biomarker association have been highlighted in red (Supplementary Data 3). In summary, synergy biomarker were derived from best performer models, and highlighted based external validation, as well as literature support.

Reporting summary. Further information on research design is available in the Nature Research Reporting Summary linked to this article.

Data availability

The data used for this study are available from the Genomics of Drug Sensitivity in Cancer (GDSC [<http://www.cancerrxgene.org/downloads/>]) repository¹², the Catalog of Somatic Mutations in Cancer (COSMIC [http://cancer.sanger.ac.uk/cell_lines/]) database⁵⁵, the European Genome-phenome Archive (EGA) EGAS00001000978, Gene Expression Omnibus (GEO) GSE68379, ArrayExpress E-MTAB-3610, Synapse database [synapse.org/DrugCombinationChallenge](https://www.synapse.org/DrugCombinationChallenge) [<https://www.synapse.org/DrugCombinationChallenge>] and the AstraZeneca Open Innovation Portal openinnovation.astrazeneca.com/data-library.html [<https://openinnovation.astrazeneca.com/data-library.html>].

Code availability

Full description and source code of all participants in this Challenge can be downloaded from [synapse.org/DrugCombinationChallenge](https://www.synapse.org/DrugCombinationChallenge) [<https://www.synapse.org/DrugCombinationChallenge>].

Received: 12 February 2018 Accepted: 1 April 2019

Published online: 17 June 2019

References

- Holohan, C., Van Schaeybroeck, S., Longley, D. B. & Johnston, P. G. Cancer drug resistance: an evolving paradigm. *Nat. Rev. Cancer* **13**, 714–726 (2013).
- Hanahan, D. & Weinberg, R. A. Hallmarks of cancer: the next generation. *Cell* **144**, 646–674 (2011).
- Dry, J. R., Yang, M. & Saez-Rodriguez, J. Looking beyond the cancer cell for effective drug combinations. *Genome Med.* **8**, 125 (2016).
- O'Neil, J. et al. An unbiased oncology drug screen to identify novel combination strategies. *Mol. Cancer Ther.* **15**, 1155–1162 (2016).
- Al-Lazikani, B., Banerji, U. & Workman, P. Combinatorial drug therapy for cancer in the post-genomic era. *Nat. Biotechnol.* **30**, 679–692 (2012).
- Bulusu, K. C. et al. Modelling of drug combination effects and applications to efficacy and toxicity: state-of-the-art, challenges and perspectives. *Drug Discov. Today* **21**, 225–238 (2016).
- Bansal, M. et al. A community computational challenge to predict the activity of pairs of drugs. *Nat. Biotechnol.* **32**, 1213–1222 (2014).

8. Gao, H. et al. High-throughput screening using patient-derived tumor xenografts to predict clinical trial drug response. *Nat. Med.* **21**, 1318–1325 (2015).
9. Saez-Rodriguez, J. et al. Crowdsourcing biomedical research: leveraging communities as innovation engines. *Nat. Rev. Genet.* **17**, 470–486 (2016).
10. Loewe, S. Effect of combinations : mathematical basis of problem. *Arch. Exp. Pathol. Pharmacol.* **114**, 313–326 (1926).
11. Di Veroli, G. Y. et al. Combeneft: an interactive platform for the analysis and visualization of drug combinations. *Bioinformatics* **32**, 2866–2868 (2016).
12. Iorio, F. et al. A Landscape of Pharmacogenomic Interactions in. *Cancer Cell* **166**, 740–754 (2016).
13. Holbeck, S. L. et al. The National Cancer Institute ALMANAC: A comprehensive screening resource for the detection of anticancer drug pairs with enhanced therapeutic activity. *Cancer Res.* **77**, 3564–3576 (2017).
14. Marbach, D. et al. Wisdom of crowds for robust gene network inference. *Nat. Methods* **9**, 796–804 (2012).
15. Parisi, F., Strino, F., Nadler, B. & Kluger, Y. Ranking and combining multiple predictors without labeled data. *Proc. Natl Acad. Sci. USA* **111**, 1253–1258 (2014).
16. Gene Ontology Consortium. Gene Ontology Consortium: going forward. *Nucl. Acids Res.* **43**, D1049–D1056 (2015).
17. Kanehisa, M., Sato, Y., Kawashima, M., Furumichi, M. & Tanabe, M. KEGG as a reference resource for gene and protein annotation. *Nucl. Acids Res* **44**, D457–D462 (2016).
18. Babur, Ö. et al. Systematic identification of cancer driving signaling pathways based on mutual exclusivity of genomic alterations. *Genome Biol.* **16**, 45 (2015).
19. Türei, D., Korcsmaros, T. & Saez-Rodriguez, J. OmniPath: guidelines and gateway for literature-curated signaling pathway resources. *Nat. Methods* **13**, 966–967 (2016).
20. López-Otín, C. & Hunter, T. The regulatory crosstalk between kinases and proteases in cancer. *Nat. Rev. Cancer* **10**, 278–292 (2010).
21. Haibe-Kains, B. et al. Inconsistency in large pharmacogenomic studies. *Nature* **504**, 389–393 (2013).
22. Dent, P., Curiel, D. T., Fisher, P. B. & Grant, S. Synergistic combinations of signaling pathway inhibitors: mechanisms for improved cancer therapy. *Drug Resist. Updat.* **12**, 65–73 (2009).
23. Eduati, F. et al. Drug Resistance mechanisms in colorectal cancer dissected with cell type-specific dynamic logic models. *Cancer Res.* **77**, 3364–3375 (2017).
24. Kirouac, D. C. et al. Clinical responses to ERK inhibition in BRAF(V600E)-mutant colorectal cancer predicted using a computational model. *NPJ Syst. Biol. Appl.* **3**, 14 (2017).
25. Klinger, B. et al. Network quantification of EGFR signaling unveils potential for targeted combination therapy. *Mol. Syst. Biol.* **9**, 673 (2013).
26. Silverbush, D. et al. Cell-specific computational modeling of the PIM pathway in acute myeloid leukemia. *Cancer Res.* **77**, 827–838 (2017).
27. Flobak, Å. et al. Discovery of drug synergies in gastric cancer cells predicted by logical modeling. *PLoS Comput. Biol.* **11**, e1004426 (2015).
28. Fallahi-Sichani, M. et al. Adaptive resistance of melanoma cells to RAF inhibition via reversible induction of a slowly dividing de-differentiated state. *Mol. Syst. Biol.* **13**, 905 (2017).
29. Margolin, A. A. et al. Reverse engineering cellular networks. *Nat. Protoc.* **1**, 662–671 (2006).
30. Lefebvre, C. et al. A human B-cell interactome identifies MYB and FOXM1 as master regulators of proliferation in germinal centers. *Mol. Syst. Biol.* **6**, 377 (2010).
31. Fakhry, C. T. et al. Interpreting transcriptional changes using causal graphs: new methods and their practical utility on public networks. *BMC Bioinforma.* **17**, 318 (2016).
32. Leiserson, M. D. M. et al. Pan-cancer network analysis identifies combinations of rare somatic mutations across pathways and protein complexes. *Nat. Genet.* **47**, 106–114 (2015).
33. Alvarez, M. J., Chen, J. C. & Califano, A. DIGGIT: a Bioconductor package to infer genetic variants driving cellular phenotypes. *Bioinformatics* **31**, 4032–4034 (2015).
34. Yi, Y. W. et al. Inhibition of the PI3K/AKT pathway potentiates cytotoxicity of EGFR kinase inhibitors in triple-negative breast cancer cells. *J. Cell. Mol. Med.* **17**, 648–656 (2013).
35. Wei, F. et al. mTOR inhibition induces EGFR feedback activation in association with its resistance to human pancreatic cancer. *Int. J. Mol. Sci.* **16**, 3267–3282 (2015).
36. Shi, X. -B. et al. Functional analysis of 44 mutant androgen receptors from human prostate cancer. *Cancer Res.* **62**, 1496–1502 (2002).
37. Gottlieb, B., Beitel, L. K., Nadarajah, A., Paliouras, M. & Trifiro, M. The androgen receptor gene mutations database: 2012 update. *Hum. Mutat.* **33**, 887–894 (2012).
38. Eisermann, K., Wang, D., Jing, Y., Pascal, L. E. & Wang, Z. Androgen receptor gene mutation, rearrangement, polymorphism. *Transl. Androl. Urol.* **2**, 137–147 (2013).
39. Carver, B. S. et al. Reciprocal feedback regulation of PI3K and androgen receptor signaling in PTEN-deficient prostate cancer. *Cancer Cell* **19**, 575–586 (2011).
40. Zhu, M. -L. & Kyprianou, N. Androgen receptor and growth factor signaling cross-talk in prostate cancer cells. *Endocr. Relat. Cancer* **15**, 841–849 (2008).
41. Meng, X. et al. ADAM17-siRNA inhibits MCF-7 breast cancer through EGFR-PI3K-AKT activation. *Int. J. Oncol.* **49**, 682–690 (2016).
42. Zheng, X. et al. ADAM17 promotes breast cancer cell malignant phenotype through EGFR-PI3K-AKT activation. *Cancer Biol. Ther.* **8**, 1045–1054 (2009).
43. Schwartz, S. et al. Feedback suppression of PI3Kα signaling in PTEN-mutated tumors is relieved by selective inhibition of PI3Kβ. *Cancer Cell* **27**, 109–122 (2015).
44. Palmer, A. C. & Sorger, P. K. Combination cancer therapy can confer benefit via patient-to-patient variability without drug additivity or synergy. *Cell* **171**, 1678–1691 (2017). e13.
45. Lopez, J. S. & Banerji, U. Combine and conquer: challenges for targeted therapy combinations in early phase trials. *Nat. Rev. Clin. Oncol.* **14**, 57–66 (2016).
46. Di Veroli, G. Y. et al. An automated fitting procedure and software for dose-response curves with multiphasic features. *Sci. Rep.* **5**, 14701 (2015).
47. Stephens, P. J. et al. The landscape of cancer genes and mutational processes in breast cancer. *Nature* **486**, 400–404 (2012).
48. Ye, K., Schulz, M. H., Long, Q., Apweiler, R. & Ning, Z. Pindel: a pattern growth approach to detect break points of large deletions and medium sized insertions from paired-end short reads. *Bioinformatics* **25**, 2865–2871 (2009).
49. Greenman, C. D. et al. PICNIC: an algorithm to predict absolute allelic copy number variation with microarray cancer data. *Biostatistics* **11**, 164–175 (2010).
50. Gautier, L., Cope, L., Bolstad, B. M. & Irizarry, R. A. Affy-analysis of Affymetrix GeneChip data at the probe level. *Bioinformatics* **20**, 307–315 (2004).
51. Du, P. et al. Comparison of Beta-value and M-value methods for quantifying methylation levels by microarray analysis. *BMC Bioinforma.* **11**, 587 (2010).
52. Kent, W. J. et al. The human genome browser at UCSC. *Genome Res.* **12**, 996–1006 (2002).
53. Jaffe, A., Nadler, B. & Kluger, Y. Estimating the accuracies of multiple classifiers without labeled data. *Artif. Intel. Stat.* **38**, 407–415 (2015).
54. Wappett, M. et al. Multi-omic measurement of mutually exclusive loss-of-function enriches for candidate synthetic lethal gene pairs. *BMC Genom.* **17**, 65 (2016).
55. Forbes, S. A. et al. COSMIC: exploring the world's knowledge of somatic mutations in human cancer. *Nucl. Acids Res.* **43**, D805–D811 (2015).

Acknowledgements

We thank the Genomics of Drug Sensitivity in Cancer and COSMIC teams at the Wellcome Trust Sanger Institute for help with the preparation of the molecular data, Denes Turei for help with Omnipath, and Katjusa Koler for help with matching drug names across combination screens. We thank AstraZeneca for funding and provision of data to the DREAM Consortium to run the challenge, and funding from the European Union Horizon 2020 research (under grant agreement No 668858 PrECISE to J.S.R.), the Joint Research Center for Computational Biomedicine (which is partially funded by Bayer AG) to J.S.R., National Institute for Health Research (NIHR) Sheffield Biomedical Research Center, Premium Postdoctoral Fellowship Program of the Hungarian Academy of Sciences. M.G lab is supported by Wellcome Trust (102696 and 206194).

Author contributions

M.P.M., D.W., T.Y., I.S.J., T.No, G.Y.D., S.F., G.S., J.G., J.R.D., and J.S.R. designed the challenge. The top-performing approach was designed by Y.G. Data analysis for the top-performing approach was conducted by M.P.M., D.W., M.M., B.S., K.C.B., J.K., M.J., R.W., T.Ng, and M.Z. The DREAM Consortium provided drug synergy and biomarker predictions, as well as method implementations and descriptions. M.P.M., D.W., M.M., T.Y., E.C.N., R.V., and M.E.A. performed analysis of challenge predictions. M.P.M., D.W., M.M., B.S., and K.C.B. interpreted the results of the challenge and performed follow-up analyses for the manuscript. E.K.Y.T., M.J.G., Z.G., and S.F. generated experimental data. M.P.M., D.W., Y.G., M.M., B.S., K.C.B., T.Y., J.K., M.J., R.W., T.Ng, M.Z., I.S.J., J.G., J.R.D., and J.S.R. wrote the manuscript. J.G., J.R.D., and J.S.R. supervised the project.

Additional information

Supplementary Information accompanies this paper at <https://doi.org/10.1038/s41467-019-09799-2>.

Competing interests: K.C.B., Z.G., G.Y.D., E.K.Y.T., S.F., and J.R.D. are AstraZeneca employees. K.C.B., Z.G., E.K.Y.T., S.F., and J.R.D. are AstraZeneca shareholders. Y.G. receives personal compensation from Eli Lilly and Company, is a shareholder of Cleerly, Inc., and Ann Arbor Algorithms, Inc. M.G. receives research funding from AstraZeneca and has performed consultancy for Sanofi. The remaining authors declare no competing interests.

Reprints and permission information is available online at <http://npg.nature.com/reprintsandpermissions/>

Journal peer review information: *Nature Communications* thanks the anonymous reviewers for their contribution to the peer review of this work.

Publisher's note: Springer Nature remains neutral with regard to jurisdictional claims in published maps and institutional affiliations.



Open Access This article is licensed under a Creative Commons Attribution 4.0 International License, which permits use, sharing, adaptation, distribution and reproduction in any medium or format, as long as you give appropriate credit to the original author(s) and the source, provide a link to the Creative Commons license, and indicate if changes were made. The images or other third party material in this article are included in the article's Creative Commons license, unless indicated otherwise in a credit line to the material. If material is not included in the article's Creative Commons license and your intended use is not permitted by statutory regulation or exceeds the permitted use, you will need to obtain permission directly from the copyright holder. To view a copy of this license, visit <http://creativecommons.org/licenses/by/4.0/>.

© The Author(s) 2019

AstraZeneca-Sanger Drug Combination DREAM Consortium

Jordi Abante¹⁸, Barbara Schmitz Abecassis¹⁹, Nanne Aben^{20,21}, Delasa Aghamirzaie²², Tero Aittokallio²³, Farida S. Akhtari²⁴, Bissan Al-lazikani²⁵, Tanvir Alam²⁶, Amin Allam²⁷, Chad Allen²⁸, Mariana Pelicano de Almeida¹⁹, Doaa Altarawy^{29,30}, Vinicius Alves³¹, Alicia Amadoz³², Benedict Anchang³³, Albert A. Antolin²⁵, Jeremy R. Ash³⁴, Victoria Romeo Aznar³⁵, Wail Ba-alawi²⁶, Moeen Bagheri³⁶, Vladimir Bajic²⁶, Gordon Ball³⁷, Pedro J. Ballester^{38,39,40,41}, Delora Baptista⁴², Christopher Bare⁴, Mathilde Bateson⁴³, Andreas Bender²⁸, Denis Bertrand⁴⁴, Bhagya Wijayawardena⁴⁵, Keith A. Boroevich⁴⁶, Evert Bosdriesz^{20,47}, Salim Bougouffa²⁶, Gergana Bounova²⁰, Thomas Brouwer⁴⁸, Barbara Bryant⁴⁹, Manuel Calaza⁵⁰, Alberto Calderone⁵¹, Stefano Calza^{52,53}, Stephen Capuzzi³¹, Jose Carbonell-Caballero⁵⁴, Daniel Carlin⁵⁵, Hannah Carter⁵⁵, Luisa Castagnoli⁵⁶, Remzi Celebi⁵⁷, Gianni Cesareni⁵⁶, Hyeokyeon Chang⁹, Guocai Chen⁵⁸, Haoran Chen⁵⁹, Huiyuan Chen⁶⁰, Lijun Cheng⁴⁵, Ariel Chernomoretz³⁵, Davide Chicco⁶¹, Kwang-Hyun Cho⁶², Sunghwan Cho⁶², Daeseon Choi⁶³, Jaejoon Choi⁶⁴, Kwanghun Choi⁹, Minsoo Choi⁶³, Martine De Cock⁶⁵, Elizabeth Coker²⁵, Isidro Cortes-Ciriano⁶⁶, Miklós Cserző^{5,6}, Cankut Cubuk⁶⁷, Christina Curtis⁶⁸, Dries Van Daele⁶⁹, Cuong C. Dang^{38,39,40,41}, Tjeerd Dijkstra⁷⁰, Joaquin Dopazo⁶⁷, Sorin Draghici^{71,72}, Anastasios Drosou⁷³, Michel Dumontier⁷⁴, Friederike Ehrhart¹⁹, Fatma-Elzahraa Eid^{29,75}, Mahmoud ElHefnawi^{76,77}, Haitham Elmarakeby^{29,75}, Bo van Engelen¹⁹, Hatice Billur Engin⁵⁵, Iwan de Esch⁷⁸, Chris Evelo¹⁹, Andre O. Falcao⁷⁹, Sherif Farag³¹, Carlos Fernandez-Lozano⁸⁰, Kathleen Fisch⁸¹, Asmund Flobak^{82,83}, Chiara Fornari¹, Amir B.K. Foroushani⁸⁴, Donatien Chedom Fotso⁸⁵, Denis Fourches⁸⁶, Stephen Friend⁴, Arnaldo Frigessi⁸⁷, Feng Gao⁸⁸, Xiaoting Gao⁸⁹, Jeffrey M. Gerold⁹⁰, Pierre Gestraud⁹¹, Samik Ghosh⁹², Jussi Gillberg⁹³, Antonia Godoy-Lorite⁹⁴, Lizzy Godynyuk¹⁹, Adam Godzik⁹⁵, Anna Goldenberg⁹⁶, David Gomez-Cabrero^{37,97}, Mehmet Gonen^{98,99}, Chris de Graaf⁷⁸, Harry Gray¹⁰⁰, Maxim Grechkin¹⁰¹, Roger Guimera^{94,102}, Emre Guney¹⁰³, Benjamin Haibe-Kains¹⁰⁴, Younghyun Han⁶², Takeshi Hase⁹², Di He¹⁰⁵, Liye He²³, Lenwood S. Heath²⁹, Kristoffer H. Hellton¹⁰⁶, Manuela Helmer-Citterich⁵⁶, Marta R. Hidalgo⁶⁷, Daniel Hidru³⁶, Steven M. Hill¹⁰⁰, Sepp Hochreiter¹⁰⁷, Seungpyo Hong¹⁰⁸, Eivind Hovig^{109,110}, Ya-Chih Hsueh³⁶, Zhiyuan Hu¹¹¹, Justin K Huang¹¹², R. Stephanie Huang¹¹³, László Hunyady^{5,6}, Jinseub Hwang¹¹⁴, Tae Hyun Hwang¹¹⁵, Woochang Hwang⁶⁴, Yongdeuk Hwang¹¹⁶, Olexandr Isayev³¹, Oliver Bear Don't Walk IV¹¹⁷, John Jack²⁴, Samad Jahandideh⁹⁵, Jiadong Ji^{118,119,120}, Yousang Jo⁶², Piotr J. Kamola⁴⁶, Georgi K. Kanev⁷⁸, Loukia Karacosta³³, Mostafa Karimi¹⁸, Samuel Kaski⁹³, Marat Kazanov^{121,122}, Abdullah M Khamis²⁶, Suleiman Ali Khan²³, Narsis A. Kiani¹²³, Allen Kim¹⁰¹, Jinhan Kim¹²⁴, Juntae Kim⁶², Kiseong Kim⁶², Kyung Kim¹²⁵, Sunkyu Kim⁹, Yongsoo Kim^{20,126}, Yunseong Kim⁶², Paul D.W. Kirk¹⁰⁰, Hiroaki Kitano⁹², Gunter Klambauer¹⁰⁷, David Knowles^{33,127}, Melissa Ko¹²⁸, Alvaro Kohn-Luque¹²⁹, Albert J. Kooistra⁷⁸, Melaine A. Kuenemann⁸⁶,

Martin Kuiper⁸², Christoph Kurz¹³⁰, Mijin Kwon⁶², Twan van Laarhoven¹³¹, Astrid Laegreid⁸², Simone Lederer¹³¹, Heewon Lee⁹, Jeon Lee¹¹⁵, Yun Woo Lee⁶³, Eemeli Lepp_aho⁹³, Richard Lewis²⁸, Jing Li⁶⁰, Lang Li¹³², James Liley¹³³, Weng Khong Lim^{134,135}, Chieh Lin¹³⁶, Yiyi Liu⁸⁹, Yosvany Lopez^{46,137,138}, Joshua Low¹⁹, Artem Lysenko⁴⁶, Daniel Machado⁴², Neel Madhukar¹³⁹, Dries De Maeyer¹⁴⁰, Ana Belen Malpartida¹⁹, Hiroshi Mamitsuka¹⁴¹, Francesco Marabita³⁷, Kathleen Marchal¹⁴⁰, Pekka Marttinen¹⁴², Daniel Mason²⁸, Alireza Mazaheri¹²³, Arfa Mehmood¹⁴³, Ali Mehreen¹⁴⁴, Magali Michaut²⁰, Ryan A. Miller¹⁹, Costas Mitsopoulos²⁵, Dezso Modos²⁸, Marijke Van Moerbeke¹⁴⁵, Keagan Moo¹⁰¹, Alison Motsinger-Reif²⁴, Rajiv Movva¹²⁷, Sebastian Muraru¹⁹, Eugene Muratov³¹, Mushthofa Mushthofa¹⁴⁶, Niranjan Nagarajan⁴⁴, Sigve Nakken¹⁴⁷, Aritro Nath¹¹³, Pierre Neuvial¹⁴⁷, Richard Newton¹⁴⁸, Zheng Ning⁵³, Carlos De Niz¹⁴⁹, Baldo Oliva¹⁵⁰, Catharina Olsen^{145,151}, Antonio Palmeri⁵⁶, Bhawan Panesar³⁶, Stavros Papadopoulos⁷³, Jaesub Park⁶², Seonyeong Park⁶³, Sungjoon Park⁹, Yudi Pawitan⁵³, Daniele Peluso⁵⁶, Sriram Pendyala¹⁵², Jian Peng¹⁵³, Livia Perfetto⁵⁶, Stefano Pirro⁵⁶, Sylvia Plevritis³³, Regina Politi³¹, Hoifung Poon¹⁵⁴, Eduard Porta⁹⁵, Isak Prellner¹⁵⁵, Kristina Preuer¹⁰⁷, Miguel Angel Pujana^{156,157}, Ricardo Ramnarine³⁶, John E. Reid¹⁰⁰, Fabien Reyat¹⁵⁸, Sylvia Richardson¹⁰⁰, Camir Ricketts¹³⁹, Linda Rieswijk^{19,159}, Miguel Rocha⁴², Carmen Rodriguez-Gonzalvez²⁵, Kyle Roell²⁴, Daniel Rotroff²⁴, Julian R. de Ruiter^{20,160}, Ploy Rukawa¹⁴⁸, Benjamin Sadacca¹⁵⁸, Zhaleh Safikhani¹⁰⁴, Fita Safitri¹⁶¹, Marta Sales-Pardo⁹⁴, Sebastian Sauer¹⁶², Moritz Schlichting¹⁹, Jose A. Seoane⁶⁸, Jordi Serra^{156,157}, Ming-Mei Shang³⁷, Alok Sharma^{46,163,164}, Hari Sharma³⁶, Yang Shen¹⁸, Motoki Shiga¹⁶⁵, Moonshik Shin⁶², Ziv Shkedy¹⁶⁶, Kevin Shopsowitz¹⁶⁷, Sam Sinai⁹⁰, Dylan Skola¹¹², Petr Smirnov¹⁰⁴, Izel Fourie Soerensen¹⁶⁸, Peter Soerensen¹⁶⁸, Je-Hoon Song⁶², Sang Ok Song¹²⁴, Othman Soufan²⁰, Andreas Spitzmueller¹⁶⁹, Boris Steipe³⁶, Chayaporn Suphavilai^{44,170}, Sergio Pulido Tamayo⁶⁹, David Tamborero¹⁷¹, Jing Tang²³, Zia-ur-Rehman Tanoli²³, Marc Tarres-Deulofeu⁹⁴, Jesper Tegner^{37,172}, Liv Thommesen⁸², Seyed Ali Madani Tonekaboni¹⁰⁴, Hong Tran²⁹, Ewoud De Troyer¹⁶⁶, Amy Truong⁴, Tatsuhiko Tsunoda^{46,137,138}, Gábor Turu^{5,6}, Guang-Yo Tzeng³⁶, Lieven Verbeke¹⁴⁰, Santiago Videla³⁵, Daniel Vis²⁰, Andrey Voronkov¹⁴⁷, Konstantinos Votis⁷³, Ashley Wang³⁶, Hong-Qiang Horace Wang¹⁷³, Po-Wei Wang¹³⁶, Sheng Wang¹⁵³, Wei Wang⁸⁸, Xiaochen Wang⁸⁹, Xin Wang⁸⁸, Krister Wennerberg²³, Lorenz Wernisch¹⁰⁰, Lodewyk Wessels^{20,21,47}, Gerard J.P. van Westen¹⁷⁴, Bart A. Westerman¹⁷⁵, Simon Richard White¹⁰⁰, Egon Willighagen¹⁹, Tom Wurdinger¹⁷⁵, Lei Xie¹⁷⁶, Shuilian Xie¹⁸, Hua Xu⁵⁸, Bhagwan Yadav¹⁷⁷, Christopher Yau¹⁷⁸, Huwate Yeerna¹⁷⁹, Jia Wei Yin³⁷, Michael Yu¹¹², MinHwan Yu⁹, So Jeong Yun¹²⁴, Alexey Zakharov¹⁸⁰, Alexandros Zamichos⁷³, Massimiliano Zanin¹⁸¹, Li Zeng⁸⁹, Hector Zenil^{123,182}, Frederick Zhang³⁶, Pengyue Zhang¹⁸³, Wei Zhang⁵⁵, Hongyu Zhao⁸⁹, Lan Zhao¹⁸⁴, Wenjin Zheng⁵⁸, Azedine Zoufir²⁸ & Manuela Zucknick¹²⁹

¹⁸Department of Electrical and Computer Engineering, Texas A&M University, College Station 77843, USA. ¹⁹Department of Bioinformatics - BiGCaT NUTRIM Maastricht University, Maastricht 6229 ER, The Netherlands. ²⁰Division of Molecular Carcinogenesis NKI, Amsterdam 1066 CX, The Netherlands. ²¹Faculty of EEMCS, Delft University of Technology, Delft 2628 CD, The Netherlands. ²²Genetics Bioinformatics and Computational Biology Virginia Tech, Blacksburg, VA 24061, USA. ²³Institute for Molecular Medicine Finland FIMM, University of Helsinki, Helsinki FI-00014, Finland. ²⁴Bioinformatics Research Center North Carolina State University, Raleigh, NC 27695-7566, USA. ²⁵The Institute of Cancer Research, London SW3 6JB, UK. ²⁶Computational Bioscience Research Center (CBRC) KAUST, Thuwal 23955, Saudi Arabia. ²⁷King Abdullah University of Science and Technology (KAUST), Thuwal 23955, Saudi Arabia. ²⁸Centre for Molecular Informatics, Department of Chemistry, University of Cambridge, Cambridge CB2 1EW, UK. ²⁹Department of Computer Science Virginia Tech, Blacksburg, VA 24061, USA. ³⁰Alexandria University, Alexandria 21500, Egypt. ³¹Eshelman School of Pharmacy, University of North Carolina at Chapel Hill, Chapel Hill 27599, USA. ³²Department of Bioinformatics, Igenomix SL, Valencia 46980, Spain. ³³Department of Radiology, Stanford University, Drive, Stanford 94305, USA. ³⁴Bioinformatics Research Center, Department of Chemistry, Department of Statistics, North Carolina State University, Raleigh, NC 27695, USA. ³⁵Leloir Institute, Buenos Aires C1405 BWE, Argentina. ³⁶University of Toronto, Toronto, ON M5S, Canada. ³⁷Unit of Computational Medicine, Department of Medicine, Solna SciLifeLab Center for Molecular Medicine Karolinska Institute, Solna SE-171 76, Sweden. ³⁸INSERM U1068, Marseille 13005, France. ³⁹Institut Paoli-Calmettes, Marseille 13009, France. ⁴⁰Aix-Marseille University, 13007 Marseille, France. ⁴¹CNRS UMR7258, Marseille 13273, France. ⁴²Centre Biological Engineering (CEB), University of Minho, Braga 4710-057, Portugal. ⁴³Institut HyperCube, Paris 92907, France. ⁴⁴Computational and Systems Biology, Genome Institute of Singapore, Singapore 138672, Singapore. ⁴⁵Indiana University School of Medicine, Indianapolis 46202, USA. ⁴⁶Center for Integrative Medical Sciences RIKEN Japan, Kobe, Hyogo 650-0047, Japan. ⁴⁷Cancer Genomics Netherlands, Utrecht 3584 CG, Netherlands. ⁴⁸Computer Laboratory, University of Cambridge, Cambridge CB3 0FD, UK. ⁴⁹Constellation

Pharmaceuticals, Cambridge 2142, USA. ⁵⁰CIMUS University of Santiago de Compostela, La Coruña 15001, Spain. ⁵¹Bioinformatics and Computational Biology Unit, Department of Biology, University of Rome Tor Vergata, Rome 00133, Italy. ⁵²Department of Molecular and Translational Medicine, University of Brescia, Brescia 25123, Italy. ⁵³Department of Medical Epidemiology and Biostatistics, Karolinska Institute, Stockholm SE-171 76, Sweden. ⁵⁴Centre de Regulacio Genomica (CRG), Barcelona Institute for Science and Technology, Barcelona 08036, Spain. ⁵⁵Department of Medicine, University of California, San Diego, La Jolla, CA 92093, USA. ⁵⁶Department of Biology, University of Rome Tor Vergata, Rome 00133, Italy. ⁵⁷Department of Computer Engineering, Ege University Turkey, Metro İstasyonu 35100, Turkey. ⁵⁸University of Texas Health Science Center, Houston 77030, USA. ⁵⁹Texas A&M University, Station, College Station, TX 77843, USA. ⁶⁰Case Western University, Cleveland 44106, USA. ⁶¹Princess Margaret Cancer Centre, Toronto M5G 2C1, Canada. ⁶²Department of Bio and Brain Engineering, Korea Advanced Institute of Science and Technology (KAIST), Daejeon 34141, South Korea. ⁶³Department of Medical Information, Kongju National University, Gongju 32588, South Korea. ⁶⁴Bio-Synergy Research Center, Daejeon 02451, Republic of Korea. ⁶⁵University of Washington Tacoma, Tacoma 98402, USA. ⁶⁶Departement de Biologie Structurale et Chimie Institut Pasteur Unite de Bioinformatique Structurale CNRS UMR, 3825 Paris, France. ⁶⁷Clinical Bioinformatic Area Fundacion Progreso y Salud CDCA Hospital Virgen del Rocío, Sevilla 41092, Spain. ⁶⁸Stanford University, Stanford 94305, USA. ⁶⁹KU Leuven, Leuven 3000, Belgium. ⁷⁰Max Planck Institute for Developmental Biology, Tuebingen 72076, Germany. ⁷¹Department of Computer Science, Wayne State University Michigan, Detroit 48202, USA. ⁷²Department of Obstetrics and Gynecology, Wayne State University Michigan, Detroit 48202, USA. ⁷³CERTH-ITI, Thessaloniki GR 5700, Greece. ⁷⁴Institute of Data Science, Maastricht University, Maastricht 6229 ER, Netherlands. ⁷⁵Al-Azhar University, Cairo 11651, Egypt. ⁷⁶National Research Centre, Cairo 12622, Egypt. ⁷⁷Nile University, Cairo 12622, Egypt. ⁷⁸Division of Medicinal Chemistry, AIMMS Vrije Universiteit, Amsterdam 1081 HZ, The Netherlands. ⁷⁹LaSIGE Faculdade de Ciências Universidade de Lisboa Portugal, Lisboa 1749-016, Portugal. ⁸⁰University of A Coruna, Coruña 15001, Spain. ⁸¹Center for Computational Biology and Bioinformatics, University of California, San Diego, La Jolla, CA 92093, USA. ⁸²Norwegian University of Science and Technology, Trondheim 7491, Norway. ⁸³St. Olav's University Hospital, Trondheim 7030, Norway. ⁸⁴Texas State University, San Marcos Texas, San Marcos 78666, USA. ⁸⁵University of Oxford, Oxford OX1 2JD, UK. ⁸⁶Bioinformatics Research Center, Department of Chemistry, North Carolina State University, Raleigh, NC 27695, USA. ⁸⁷Oslo Centre for Biostatistics and Epidemiology, University of Oslo and Oslo University Hospital Norway, Oslo 0317, Norway. ⁸⁸Department of Biomedical Sciences, City University of Hong Kong, Hong Kong 999077, Hong Kong. ⁸⁹Yale University, New Haven 06520, USA. ⁹⁰Program for Evolutionary Dynamics, Harvard University, Cambridge 02138, USA. ⁹¹Institut Curie Inserm U900, Paris 75248, France. ⁹²The Systems Biology Institute Tokyo, Tokyo 141-0022, Japan. ⁹³Department of Computer Science Aalto University, Espoo 02150, Finland. ⁹⁴Departament d'Enginyeria, Química Universitat Rovira i Virgili, Tarragona 43007, Spain. ⁹⁵Sanford Burnham Prebys Medical Discovery Institute, Jolla 92037, USA. ⁹⁶Hospital for Sick Children, Toronto, Ontario M5G 1X8, Canada. ⁹⁷Mucosal and Salivary Biology Division King's College London Dental Institute, London SE1 9RT, UK. ⁹⁸College of Engineering, Koc University, Istanbul 34450, Turkey. ⁹⁹School of Medicine, Koc University, Istanbul 34450, Turkey. ¹⁰⁰MRC Biostatistics Unit University of Cambridge, Cambridge CB2 0SR, UK. ¹⁰¹University of Washington, Seattle, WA 98195, USA. ¹⁰²ICREA, Barcelona 08010, Spain. ¹⁰³Joint IRB-BSC-CRG Program in Computational Biology Institute for Research in Biomedicine, Barcelona 08028, Spain. ¹⁰⁴Princess Margaret Cancer Centre, University Health Network, Toronto, M5G 2C1 ON, Canada. ¹⁰⁵Ph.D. Program in Computer Science, The Graduate Center, The City University of New York, New York 10016, USA. ¹⁰⁶Department of Mathematics University of Oslo, Oslo 0371, Norway. ¹⁰⁷Institute of Machine Learning Johannes Kepler University Linz, Linz 4040, Austria. ¹⁰⁸University of Wisconsin, Madison 53706, USA. ¹⁰⁹Department of Tumor Biology Institute for Cancer Research, Oslo University Hospital Norway, Oslo 0424, Norway. ¹¹⁰Department of Informatics University of Oslo, Oslo 0316, Norway. ¹¹¹Wellcome Trust Centre for Human Genetics University of Oxford, Oxford OX3 7BN, UK. ¹¹²Bioinformatics and Systems Biology Program, University of California, San Diego, La Jolla, CA 92093, USA. ¹¹³University of Minnesota, Minneapolis 55455, USA. ¹¹⁴Department of Computer Science and Statistics, Daegu University, Daegu 38453, South Korea. ¹¹⁵Department Bioinformatics, University of Texas Southwestern Medical Center, Dallas, TX 75390, USA. ¹¹⁶Department of Computer Science, The University of Suwon, Suwon 16499, Republic of Korea. ¹¹⁷Department of Biomedical Informatics, Columbia University in the City of New York, New York 10032, USA. ¹¹⁸School of Statistics Shandong, University of Finance and Economics, Jinan 250000, China. ¹¹⁹Department of Computer Science, Hunter College, The City University of New York, New York, NY 10065, USA. ¹²⁰Department of Biostatistics, School of Public Health Shandong University China, Shandong 250012, China. ¹²¹Skolkovo Institute of Science and Technology, Moscow 121205, Russia. ¹²²A.A.Kharkevich Institute for Information Transmission Problems, Moscow 127051, Russia. ¹²³Algorithmic Dynamics Lab Unit of Computational Medicine, Department of Medicine Solna, SciLifeLab Center for Molecular Medicine Karolinska Institute, Solna SE-171 76, Sweden. ¹²⁴Standigm Inc, Seoul 06250, Korea. ¹²⁵Department of Bioengineering, University of Washington, Seattle 98195, USA. ¹²⁶Division of Oncogenomics NKI, Amsterdam 1066 CX, The Netherlands. ¹²⁷Department of Genetics, Stanford University, Stanford 94305, USA. ¹²⁸Department of Cancer Biology, Stanford University Stanford, Stanford 94305, USA. ¹²⁹Oslo Centre for Biostatistics and Epidemiology, Department of Biostatistics, University of Oslo, Oslo 0317, Norway. ¹³⁰Helmholtz Zentrum Munchen Institute of Health Economics and Health Care Management, Neuherberg 85764, Germany. ¹³¹Data Science Radboud University, Nijmegen 6525, Netherlands. ¹³²The Ohio State University College of Medicine, Department of Biomedical Informatics, Columbus 43210, USA. ¹³³Department of Medicine, University of Cambridge, Cambridge CB2 0SP, UK. ¹³⁴Centre for Computational Biology Duke-NUS, Medical School Singapore, Singapore 169857, Singapore. ¹³⁵SingHealth Duke-NUS Institute of Precision Medicine Singapore, Singapore 169857, Singapore. ¹³⁶Carnegie Mellon University, Pittsburgh 15213, USA. ¹³⁷Department of Medical Science, Mathematics Medical Research Institute Tokyo Medical and Dental University, Tokyo 113-8510, Japan. ¹³⁸CREST JST, Tokyo 102-0076, Japan. ¹³⁹Weill Cornell Medicine, New York, NY 10065, USA. ¹⁴⁰Ghent University, Gent 9000, Belgium. ¹⁴¹Bioinformatics Center Institute for Chemical Research Kyoto University, Kyoto 611-0011, Japan. ¹⁴²Helsinki Institute for Information Technology HIIT, Department of Computer Science, Aalto University Finland, Espoo 02150, Finland. ¹⁴³University of Turku, Turku 20500, Finland. ¹⁴⁴Helsinki University, Helsinki 00100, Finland. ¹⁴⁵Interuniversity Institute of Bioinformatics in Brussels, Ixelles 1050, Belgium. ¹⁴⁶Ghent University Bogor Agricultural University, Gent 9000, Belgium. ¹⁴⁷Institut de Mathematiques de Toulouse, Université Paul Sabatier, Toulouse 31400, France. ¹⁴⁸University of Cambridge, Cambridge CB2 8PQ, UK. ¹⁴⁹Texas Tech University, Lubbock 79409, USA. ¹⁵⁰Structural Bioinformatics Group GRIB IMIM, Department of Experimental and Life Sciences, Universitat Pompeu Fabra Barcelona, Catalonia 08041, Spain. ¹⁵¹Machine Learning Group (MLG), Department d'Informatique, Université libre de Bruxelles (ULB), Brussels 1050, Belgium. ¹⁵²Harvard University, Cambridge 02138, USA. ¹⁵³University of Illinois at Urbana-Champaign Urbana, Champaign 61820, USA. ¹⁵⁴Microsoft Research Redmond, Redmond 98052, USA. ¹⁵⁵Cambridge Rindge and Latin High School, Cambridge 02138, USA. ¹⁵⁶Catalan Institute of Oncology (ICO), Barcelona 199 08908, Spain. ¹⁵⁷Bellvitge Biomedical Biomedical Research Institute (IDIBELL), Barcelona 199 08908, Spain. ¹⁵⁸Institut Curie RT2 Lab, Paris 75248, France. ¹⁵⁹Division of Environmental Health Sciences, School of Public Health, University of California, Berkeley, CA 94720, USA. ¹⁶⁰Division of Molecular Pathology NKI, Amsterdam 1066 CX, The Netherlands. ¹⁶¹Kyungpook National University, Daegu 41566, South Korea. ¹⁶²FOM University of Applied Sciences, Essen 45127, Germany. ¹⁶³Institute for Integrated and Intelligent Systems Griffith University, Mount Gravatt, QLD 4111, Australia. ¹⁶⁴University of the South Pacific Fiji, Suva, Fiji. ¹⁶⁵Department of Electrical Electronic and Computer Engineering, Gifu University, Gifu 501-1193, Japan. ¹⁶⁶Center for Statistics, Hasselt University Belgium, Hasselt 3590, Belgium. ¹⁶⁷Faculty of Medicine, University of British Columbia, Kelowna V1Y 1T3, Canada. ¹⁶⁸Center for Quantitative Genetics and Genomics, Department of Biology and Genetics, Aarhus

University, Aarhus 8000, Denmark. ¹⁶⁹Technische Universitat Munchen, München 80333, Germany. ¹⁷⁰Department of Computer Science, National University of Singapore, Singapore 117417, Singapore. ¹⁷¹Research Unit on Biomedical Informatics, University Pompeu Fabra UPF, Barcelona 08041, Spain. ¹⁷²Biological and Environmental Science and Engineering, Division KAUST, Thuwal 23955, Saudi Arabia. ¹⁷³Cancer Hospital of Chinese Academy of Sciences, Hefei 230031, China. ¹⁷⁴Drug Discovery and Safety Leiden, Academic Centre for Drug Research, Leiden University, Einsteinweg 55, Leiden 2333 CC, The Netherlands. ¹⁷⁵Department of Neurosurgery, Cancer Center, Amsterdam 1012 WX, The Netherlands. ¹⁷⁶Department of Computer Science, Hunter College and The Graduate Center, The City University of New York, New York, NY 10016, USA. ¹⁷⁷Hematology Research Unit Helsinki, Department of Clinical Chemistry and Hematology, University of Helsinki and Helsinki University Hospital Comprehensive Cancer Center, Helsinki 00029, Finland. ¹⁷⁸Institute of Cancer and Genomic Sciences, University of Birmingham, Birmingham B15 2SY, UK. ¹⁷⁹University of California, San Diego, SD 92093, USA. ¹⁸⁰National Center for Advancing Translational Sciences National Institutes of Health, Rockville, MD 20892, USA. ¹⁸¹Universidad Politecnica de Madrid, Madrid 28040, Spain. ¹⁸²Oxford Immune Algorithmics Ltd, Oxford RG1 3EU, UK. ¹⁸³Indiana University - Purdue University, Indianapolis 47907, USA. ¹⁸⁴Department of Electronic Engineering, City University of Hong Kong, Hong Kong 999077, Hong Kong